Protolith of ultramafic rocks in the Kluane Schist, Yukon, and implications for arc collisions in the northern Cordillera

Dante Canil, Stephen T. Johnston, Rameses J. D'Souza, Larry M. Heaman

2015

https://doi.org/10.1139/cjes-2014-0138

Canadian Journal of Earth Sciences
Revue canadienne des sciences de la Terre

Protolith of ultramafic rocks in the Kluane Schist, Yukon, and implications for arc collisions in the northern Cordillera

Journal:	*Canadian Journal of Earth Sciences*
Manuscript ID:	Draft
Manuscript Type:	Article
Date Submitted by the Author:	n/a
Complete List of Authors:	Canil, Dante; School of Earth and Ocean Sciences Johnston, Stephen; Univ. Victoria, Earth Ocean Sci. D'Souza, Rameses; Univ. Victoria, Earth Ocean Sci. Heaman, Larry; Univ. Alberta, Earth and Atmosphere
Keyword:	ultramafic, geochemistry, petrology, Yukon, Cordillera

Protolith of ultramafic rocks in the Kluane Schist, Yukon, and implications for arc collisions in the northern Cordillera

Dante Canil[a*], Stephen T. Johnston[a], Rameses J. D'Souza[a], Larry M. Heaman[b]

[a]School of Earth and Ocean Sciences
University of Victoria
3800 Finnerty Rd., Victoria, B.C., V8W 3P6

[b]Department of Earth and Atmospheric Sciences
University of Alberta
Edmonton, Alberta T6G 2E3

*corresponding author: dcanil@uvic.ca ph 250 472 4180 fx 250 721 6200

Abstract

Mafic and ultramafic rocks crop out as decimeter to centimeter sized bodies of antigorite-talc-olivine (±orthopyroxene) and lesser mafic chlorite-amphibole schist interleaved in the mainly pelitic Kluane Schist of southern Yukon. The metamorphic assemblages in ultramafic rocks exposed at Doghead Point overprint two generations of cleavage and are consistent with metamorphism reaching > 550ºC (talc + olivine) and > 750ºC (olivine + enstatite) in the (hot side up) contact aureole of the Eocene Ruby Range batholith. The bulk rock major and trace element patterns in the ultramafic rocks (> 40 wt% MgO, Mg/(Mg+Fe) > 0.90) are unlike residual mantle from partial melting in any geologic setting (i.e. ophiolite, orogenic massif, abyssal ocean floor), but are consistent with an intrusive origin as cumulate peridotite-pyroxenite from arc magmas. Identical trace element concentrations and patterns are observed in several late Triassic basalts, pyroxenites and websterites occurring to the southwest in Stikinia (present coordinates). The highly discordant U-Pb zircon date for one antigorite – talc - olivine schist sample (200 – 210 Ma) is within the range of U-Pb zircon ages for late Triassic Lewes River/ Stuhini Group and Hotailuh batholith in northern Stikinia (200 –208 Ma, 216 - 220 Ma). When combined with other published age information, the ultramafic rocks in the Kluane Schist are interpreted as knockers of deeper arc mafic/ultramafic intrusive rocks introduced to the Kluane fore arc basin between 95 - 82 Ma by exhumation along shear zones in northwestern Stikinia, most likely the re-activated Llewellyn Fault. The Kluane Schist represents a west-facing fore arc basin bordered to the east by arc-parallel strike slip fault(s) that served as a cogent mechanism for imbricating large knockers into the accretionary prism.

Introduction

Subduction, subcretion and collisions that involve volcanic arcs is an underlying theme in the story of nearly all mountain belts. In the northern Cordillera of western North America (Fig. 1), it was these processes that were responsible for construction of the collage of juvenile crust that ultimately built the North American continent westward (Gabrielse, 1991). In southwest Yukon, repeated cycles of arc magmatism, collision and sedimentation has resulted in a distinct pattern of westward-younging geological belts. Using a compilation of regional structural data, the tectonic history of the region was re-interpreted by Johnston and Canil (2007) to be a crustal section on the order of 40 km thick that youngs and becomes more juvenile with depth (Johnston and Canil, 2007). At least two episodes of arc magmatism in the Jurassic and Eocene are recorded by the intrusion of sill-like calc-alkaline batholiths. Intrusion of the Eocene batholith, referred to as the Ruby Range batholith, gave rise to an inverted metamorphic gradient in the underlying pelitic rocks of the Kluane Schist (also referred to as 'Kluane metamorphic assemblage' – Mezger, 2001a,b), which originally consisted of sediment deposited in either a back- or fore-arc basin of the subduction zone that lay outboard of the belt of arc plutons (Mezger et al, 2001a,b). Eocene contact metamorphism post-dated and overprinted a pre-existing metamorphic assemblage that recorded prograde burial and heating (Mezger et al 2001 a,b).

In this study, we undertake a detailed examination of the petrology and geochemistry of ultramafic rocks that occur throughout the Kluane Schist. The general occurrence of these rocks was first described by Templeman-Kluit (1974). Mezger (2000), based on more detailed mapping, surmised that they were 'Alpine type'

fragments of oceanic crust, implying that they had been tectonically interleaved with the adjacent sediments. The metamorphic history bears on the hydration and dehydration of the ultramafic rocks through the burial and exhumation history of subduction and collision and re-heating. The protolith of the ultramafic rocks is herein examined to explain their occurrence in a dominantly metasedimentary package, and to test the ophiolite model. Our results show demonstrate that these rocks originated as cumulates within arc plutons, show that they were derived as olistoliths from previously accreted arcs within the northern Cordillera, and place constraints on the origin and subsequent tectonic history of the Kluane basin, and adjacent portions of the northern Cordillera.

Geology

The Cordillera in Southwest Yukon exposes a crustal section from east to west consisting of: (1) Whitehorse Trough – a Jurassic arc and arc-derived sediments, (2) Aishihik assemblage - a Devonian-Mississippian arc plutonic and metamorphic assemblage, (3) Ruby Range batholith- an extension of the Eocene Coast Batholith to the south, (4) Kluane Schist – a Jurassic-Cretaceous arc-marginal metasedimentary unit, and (5) Dezedeash Group – a Jurassic-Cretaceous sequence of arc-derived greywackes (Johnston and Canil, 2007). The latter two units are divided by the Denali fault, a major dextral strike slip fault of the region (Figs. 1,2). Both the Jurassic Aishihik batholith and Eocene Ruby Range batholith are synkinematic tabular intrusions that left inverted metamorphic gradients on their country rocks to the west (Erdmer and Mortensen, 1993; Johnston and Erdmer, 1995).

The Kluane Schist strikes northwest along a belt 30 km wide by 160 km long northeast of the Denali Fault. The metasedimentary rocks are graphitic pelites

metamorphosed from lower greenschist to upper amphibolite facies, with metamorphic grade decreasing to the southwest. The earlier regional metamorphism is overprinted by a contact metamorphic aureole defined by isograds for garnet, staurolite, andalusite, cordierite and sillimanite (Mezger et al 2001; Erdmer and Mortensen, 1993). The ages of deposition are constrained by detrital zircons to be younger than 95 Ma, but older than 82 Ma, the oldest metamorphic age (Israel et al, 2011).

Doghead Point Ultramafics

Ultramafic rocks are interleaved within the metapelites as meter to kilometer sized bodies (Mezger, 2000). Our study focussed on a ~ 3km wide exposure of ultramafic rocks at Doghead Point, and near the Talbot Arm of Kluane Lake near the contact with Ruby Range batholith to the north (Fig. 3). Ultramafic rocks exposed along a west-striking ridge are rusty brown to grey green weathering in outcrop. The rocks are mostly talc-serpentine- schist with cm- to meter sized units of interfoliated chlorite-amphibole schist (Fig. 4a). Both rock types show a well-developed crenulation cleavage, overprinted by porphyroblasts of cm-sized olivine in serpentine-talc schist, or of amphibole in chlorite schists which are obvious even in outcrop (Fig. 4 b,c,d). Compositional heterogeneity in the protolith is shown by well-defined mm- to cm sized layers of talc versus chlorite dominated assemblage, appearing as dark and light layers, that can be tightly folded (Fig. 4e,f). Magnetism varies on a hand sample scale. Olivine- and chlorite- bearing portions of the rock are magnetic, while those dominated by talc are weakly to non-magnetic.

Serpentine defines a dominant cleavage that is overgrown by blades of talc (Fig. 5 a,b) some of which reach cm size. Olivine porphyroblasts overgrow serpentine and talc and can reach 3 cm in size (Fig. 4c). In some samples orthopyroxene and olivine

completely overgrow both talc and/or serpentine to form a granoblastic peridotite with little serpentine or no talc remaining (Fig. 5c). Olivine porphyroblasts can be seen to pseudomorph the crenulation cleavage defined by talc and both it and orthopyroxene overprint the cleavage (Fig. 5abc). Tremolite and minor carbonate can also be present in some samples. Magnetite is present only with later serpentine forming in microcracks of the olivine porphyroblasts. In chlorite schists, 0.2 to 1 mm laths of chlorite define a matrix overgrown by euhedral porphyroblasts of amphibole (Fig. 5d) and in some cases magnetite. Some of the metamorphic amphibole overgrows primary relic (igneous) 0. 5 – 2.0 mm grains of subhedral amphibole or pyroxene.

Mineral Chemistry

Mineral chemical analyses from four samples representative of the serpentine-talc and chlorite schists (Table 1) were obtained by electron microprobe (EMP) using methods as described in Larocque and Canil (2010). In talc-serpentine schist, talc or tremolite have highest Mg#, followed by olivine and orthopyroxene and chlorite. Olivine is rich in forsterite, and high Mn and Ni as is typical of other metamorphic olivine. Ilmenite and rutile are recognized in one sample.

In the mafic schists chlorite is high in Al and has high Mg#. The relic igneous pyroxenes and amphibole in these rocks are augite, pigeonite and magnesio-hornblende, respectively, and have lower Al but higher Mg# than the amphibole porphryoblasts which are Tschermakite.

Geochemistry

Bulk rock analyses were performed on samples of chlorite- and talc-serpentine schists. Major elements were determined by XRF on fused beads at McGill University and

ActLabs (Toronto). Trace element were determined on whoel rock powders by solution nebulisation ICPMS at UVic. Methods for both the McGill and UVic analyses are given in Larocque and Canil (2010). Duplicate samples of a talc-serpentine schist show reproducibility on trace elements (Table 2). Bulk C or S for some samples were determined by LECO analysis at McGill University.

Three samples of chlorite schist are broadly mafic or basaltic in SiO2 content but with anomalously high MgO (18 – 28 wt%) compared to typical basalts. Three of the four rocks have Mg# of ~ 0.76, on the upper end for most basalts, but are lower in Al. One sample (containing magnetite porphyroblasts) is anomalously low in Si and rich in Fe and Al (Table 2).

The talc-serpentine schists are ultramafic in composition, with MgO > 40 wt% and Mg# > 0.9. These rocks are strongly depleted in Al_2O_3 (< 3 wt%) and CaO (< 1 wt%) but have higher than normal Si for their Mg content than present in other ultramafic rocks such as mantle peridotites (Fig. 6). Both the mafic and ultramafic schists are all low in alkalies (Table 2).

The ultramafic schists are enriched in compatible trace elements Cr and Ni and depleted in mildly incompatible elements such as Cu, S, V and Sc relative to primitive mantle (Fig. 7). Unlike other mantle peridotites, in the Kluane schist the variation of Sc shows no correlation with V but a good negative correlation with Cr (Fig. 8).

Trace element abundances in chlorite schists are one to two orders of magnitude higher than in the ultramafic schists but normalized element patterns are strikingly similar, with both rock types showing a pronounced depletion in Zr and Hf and enrichment in Ni (Fig. 9). The chlorite schists also show negative Ti anomalies, whereas

the talc serpentine schists show positive anomalies that are strong for Pb and subtle for Sr. Trace element concentrations in the Kluane ultramafic rocks are an order of magnitude higher compared to mantle peridotite residues from ophiolite at a similar (Mg#), and the latter have no negative Zr and Hf anomalies.

Geochronology

Although most of the samples are ultramafic, the high Zr content observed in one sample GS01-12 near Talbot Arm (Fig. 3, Table 2) encouraged us to attempt age dating by U-Pb zircon methods. U-Pb zircon dating for this sample at the University of Alberta followed procedures described in Heaman et al. (2002) with dates calculated using the decay constants $^{238}U=1.55125E^{-10}$ and $^{235}U=9.8485E^{-10}$ a^{-1} (Jaffey et al., 1971). All errors are quoted at the 95% level of confidence (Table 3).

Three fractions of light yellow to colourless zircon were extracted. Fraction #1 occurs as fragments with low U contents and a Th/U ratio of 0.36 ratio consistent with an igneous origin. This fraction produces the most concordant age (13% discordant), with a $^{206}Pb/^{238}U$ of 202 Ma. The two remaining fractions have much lower Th/U typical of metamorphic zircon, and are highly discordant. Fraction #2 contains shards with a $^{206}Pb/^{238}U$ age of 272 Ma, and is the most discordant. Fraction #3 occurs as large fragments with a $^{206}Pb/^{238}U$ age of 203.9, not unlike fraction #1, but is also strongly discordant (Fig. 10).

Discussion

Metamorphism

The pelitic units of the Kluane Schist have mappable isograds over a broad area (Mezger et al, 2001), and serve as a template to compare with the metamoprhic assemblages of the

interfoliated ultramafic rocks. Mezger et al (2001a) used garnet and plagioclase zoning patterns to show a first regional metamorphic event in the Kluane Schist with peak conditions of about 0.7 GPa and 500ºC. This regional event is then overprinted by later contact metamorphism caused by intrusion of the Ruby Range batholith, producing an aureole at least 6 km wide. Closely spaced isograds in the pelites are mapped in detail within 4 km of the contact with the batholith, 20 km southeast of the Doghead Point ultramafics. Mineral assemblages in the pelites (Sillimanite+Hercynite) record conditions of at least 750ºC at 0.5 GPa within 4 km of the batholith contact (Mezger et al, 2001a).

The metamorphic reactions in the serpentinite system are well-studied by experiment and in classical field examples (Trommsdorf and Evans, 1972; Frost, 1975; Evans, 1977). Given the low CaO and CO_2 content of the Kluane ultramafic rocks, the appearance of serpentine (Antigorite – Atg), talc (Tlc), olivine (Ol) and orthopyroxene (Opx) in these rocks can be described by a series of reactions in the $MgO – SiO_2 – H_2O$ system:

$$Atg <=> Ol + Tlc + H_2O \quad [1]$$

The formation of En during dehydration depends on pressure. At low pressure:

$$Ol + Tlc <=> Opx + H_2O \quad [2]$$

whereas at higher pressures:

$$Atg <=> Ol + Opx + H_2O \quad [3]$$

The appearance of tremolite in one rock may be due to a higher CaO content, and attributed to the reaction:

$$Atg + Di <=> Trem + Ol + H_2O$$

There is some uncertainty in the exact P-T topology of reactions due to inconsistencies in experimental and thermodynamic data (Trommsdorff et al 1998). The exact pressure between reaction [2] and [3] is not constrained but likely near 1.5 GPa (Pawley, 1998).

Because the Kluane Schist has suffered first regional then contact metamorphism, the challenge is to unravel what part of the metamorphic assemblage in the ultramafic rocks was generated first, during deformation, and which part later and static. For example, at conditions of regional metamorphism inferred for the Kluane Schist pelites (to 500ºC, 0.7 GPa), both ol and Tlc could be produced by burial and heating of Atg, but later contact metamorphism to those temperatures could also produce that same assemblage.

Because Tlc and Ol overgrow the crenulated foliation of the rocks (Fig. 5a,b), we infer that foliation was produced during regional metamorphism and deformation of original serpentinites. The phase diagram of Pawley (1998) shows the formation of talc would require temperatures of at least 550ºC at the pressures of ~ 0.7 GPa inferred for regional metamorphism of the Kluane Schist (Mezger et al, 2001).

In contrast, the formation of Opx and elimination of Tlc by reaction [2] in rocks immediately at the contact with the Ruby Range batholith (Fig. 5d) requires temperatures of greater than 700ºC, consistent with the isograds in pelites within 4 km of the batholith produced by contact metamorphism. Orthopyroxene could also form directly from serpentinite by reaction [3] but only at pressure above 1.5 GPa, which is untenable given the much lower pressures inferred for the pelites at the edge of the batholith.

Anthophyllite can form in metamorphosed ultramafic protoliths (Evans, 1977), but is notably absent in the Kluane ultramafic rocks, likely due to the protolith having

Mg# > 0.9 (Frost, 1975), as is observed in the bulk rock samples (Table 2), kinetics, or a narrow stability field (Evans, 1977). The minor Cr-rich magnetite present in the ultramafic rocks is likely a product of Cr-spinel that altered to 'ferritchromit' during serpentinization of the original protolith. Other minor phases such as ilmenite are common in ultrabasites, and are possibly related to breakdown of earlier clinohumite.

The mafic chlorite schists interleaved with the talc-serpentine schists contain no quartz or plagioclase, and they cannot be compared to other typical metamorphic assemblages in metabasites for which metamorphic grade has been studied extensively (Liou et al, 1974). The Na-bearing pyroxene and high -Mg amphibole in these rocks is interpreted to be relic igneous phases based on its anhedral ragged crystal outlines, higher Mg# and low Al compositions (Table 1). Both of the latter minerals are overgrown by metamorphic chlorite and/or Tschermakite amphibole. In protoliths poor in SiO_2, chlorite can exist over a wide range of conditions, with increasing Al with temperature when buffered by two or more Mg-silicates (Frost, 1975). The high Al content of the chlorite is suggestive of high temperatures possibly achieved during regional metamorphism of the enveloping pelites in the Kluane Schist. An upper stability limit for chlorite is about 650ºC (Massonne, 1989). The Tschermakite porphyroblasts overgrowing chlorite likely grew above this temperature by contact metamorphism. Magnetite porphryoblasts also likely formed by contact metamorphism of a phyllosilicate-rich protolith, as observed in steatites at Serro, Minas Gerais (Doriguetto et al, 2003).

Protolith for Mafic/Ultramafic Rocks

The major and trace element chemistry can be used to determine the protolith of the mafic and ultramafic rocks in the Kluane Schist with the caveat that some elements may

have been lost or gained during two periods of metamorphism. Surface weathering and serpentinization of ultramafic rocks is often isochemical, adding only H_2O (Coleman and Keith, 1971). Marine weathering of peridotite on the seafloor may leach Mg relative to Si (Snow and Dick, 1995). Higher temperature hydrothermal metamorphism of both mafic and ultramafic rocks can mobilize Ca, Na and K and in some cases Mg and Si (Pearce and Cann, 1973). The remarkably coherent trend of MgO with Cu and S, two rather mobile elements in weathering and hydrothermal metamorphism (Fig. 7a) suggest that original relative abundances of chalcophile (Cu, Zn, Pb) or lithophile minor and trace elements (Ni, Cr, V, Sc) in the ultramafic rocks have been preserved during metamorphism. Two periods of metamorphism have presumably disturbed large ion lithophile elements, but following work of others (Jenner, 1996) we assume these processes have not disturbed relative concentrations of the less mobile REE or HFSE elements of the bulk rocks.

The protolith of what are now the antigorite talc olivine schists prior to serpentinization and metamorphism was peridotite that was either: (1) mantle rock residual from partial melting, or (2) cumulate plutonic rock formed by accumulation of olivine and pyroxenes. Both of these two types of peridotite protoliths are typified by high MgO content and high Mg# and can occur in a variety of geologic settings (cf. DenTex, 1969). Mezger (2000) suggested the Kluane ultramafic rocks were of 'Alpine-type' or ophiolite and represented oceanic crust that floored a fore-arc basin. The trends of Mg, Si and Al in residual mantle peridotite lithosphere as a function of partial melting and basalt extraction are well known (Jagoutz et al, 1979; Palme and O'Neill, 2004) as exemplified in a large database of ophiolite or orogenic massif peridotites plotted in

Figure 6. During partial melting, Al decreases and Mg increases to form a depleted residue; the opposite trend can occur during refertilization of mantle lithosphere (Leroux et al, 2007). The Kluane ultramafic rocks are displaced from the peridotite residue/refertilization trend and distinct in having a flat trend on this plot, with low Mg/Si. The rocks are richer in pyroxene component than most mantle peridotite residues. Although a small population of orogenic massif and ophiolite peridotite samples lie along the orthopyroxene-rich end of a tieline with olivine in Figure 6, this trend is due to a sampling bias of pyroxene-rich banding well known in ophiolite mantle exposures (Canil and Lee, 2009).

The concentration of compatible and incompatible trace elements also differs for the Kluane ultramafic rocks when compared with peridotite melting residues. For example, using mildly incompatible Sc as a depletion index, the trends of Cr and V in mantle peridotite residues differs greatly from those observed in the Kluane ultramafic rocks (Fig. 8). During partial melting at low pressures, the bulk D_{Cr} residue/melt is ~1 (Liang and Elthon, 1990; Canil, 2004), making Cr concentration in the residue fairly constant during depletion, and loss of Sc to the melt. In contrast, the Cr levels in the Kluane ultramafic rocks strongly increase with decreasing Sc (Fig. 8b), suggesting a strongly compatible behaviour, similar to Ni. The latter trend for Cr can be expected for crystal fractionation/accumulation, but is atypical of melt extraction in the mantle.

The covariance of Sc and V during magma generation in the mantle has been well quantified as function of oxygen fugacity of melting (Canil, 2004; Lee et al, 2005). In terrestrial cases these two elements are mildly incompatible and follow one another closely, and have a similar bulk D (~ 0.1) and resulting in a colinear trend again

exemplified by the ophiolite peridoite residues (Fig. 8a). On the other hand, the Kluane ultramafic rocks display nearly constant V with decreasing Sc, a trend that is obtuse to the trend of natural mantle melting residues (Fig. 8a). The trend of increasing V/Sc with depletion of Sc shown for the Kluane rocks can only be explained by melting at geologically unreasonable oxygen fugacities (lower than FMQ-3 , where FMQ is the fayalite-magneite-quartz oxygen buffer – Lee et al, 2005).

The incompatible element concentrations and patterns in the Kluane ultramafic rocks also differ markedly from mantle peridotite residues. For a given MgO content, the Kluane samples have one to two orders of magnitude higher incompatible element concentrations than melting residues (Fig. 7, 9). Absolute concentrations of incompatible elements, even in harzburgitic rocks, can vary with mantle metasomatism, or by distrubrance during surface processes and emplacement of mantle peridotites into the crust (Gruau et al 1991, 1998). In this regard, element *patterns* of immobile elements are more important for disturbed rocks. The Kluane ultramafic rocks have depletions in Zr and Hf that are not observed in natural peridotite residues (Fig. 9). The relative concentrations of the latter elements cannot be disturbed by metamorphism, and must be a primary imprint of their geochemistry (Jenner, 1996; Munker et al 2004).

Indeed, the Kluane ultramafic rocks parallel their mafic counterparts by having trace element patterns with depletions in Zr, Hf or Ti and enrichments in Pb, Sr or LIL - the hallmark of arc magmas (Fig. 9). The volumetrically smaller mafic rocks (chlorite - amphibole schists) interleaved with the peridotites at Doghead Point are notably more Mg-rich and Si-poor than typical basalts, and have variations in Al, Fe at a given Mg or Si content that makes them strikingly similar to igneous/cumulate pyroxenites. The

chemical trends of the mafic and ultramafic rocks are co-linear with amphibole peridotite-pyroxenite cumulates known from arcs (Fig. 11). Interestingly, the Kluane mafic rocks also have trace element abundances and patterns that are identical to those of arc-related cumulate rocks exposed elsewhere in the northern Cordillera (Fig. 9). These geochemical similarities are fortified by age relations and regional geologic setting, and further elucidate the source and origin of mafic/ultramafics rocks in the Kluane Schist.

Implications for Arc Collision Exhumation in Northern Cordillera

Intrusive pyroxenite and peridotite is known in the lower to mid crust of arc crustal sections as the plutonic complement of more evolved andesitic magmas produced during crystallization of primary arc basaltic magma (DeBari and Coleman, 1989; Greene et al, 2006; Jagoutz et al, 2007; Larocque and Canil, 2010). Arc-related pyroxenites and related mafic and ultramafic rocks are known along the margins of Stikinia, an accreted oceanic arc in the northern Cordillera. Pyroxenite and gabbro with age of 208 Ma related to the Lewes River arc are exposed in southwestern Yukon by exhumation along the Tally Ho shear zone (Tizzard et al, 2009), an east-verging thrust fault which follows the northwestern margin of Stikinia 50 km southeast of the Kluane Schist (present coordinates). Along the northeastern margin of Stikinia and south of the King Salmon thrust, arc-related volcanic rocks of the Stuhini Group occur with ages of 200 – 210 Ma (Mortensen et al, 1995). Near Dease Lake, clinopyroxenite, websterite and hornblendite phases of the Hotailuh batholith are exposed. Crosscutting relations and geochronology constrain the Beggerlay Creek and Gnat Lake mafic/ultramafic phases of that batholith to ages of 220 to 216 Ma (van Straaten et al, 2012). Rocks from these regions have trace element patterns identical to those of the Kluane mafic and ultramafic rocks (Fig. 9).

The Kluane ultramafic rock from Talbot Arm in our study produced an imprecise U-Pb zircon date of ~ 200 – 210 Ma (Table 2, Fig. 10). Nevertheless, the date for this sample matches the more precise ages for other Kluane Schist ultramafic rocks (205.9±0.4 and 206 ±3.2 Ma - M. Escaloya, as cited in Stanley(2012)). Those ages for Kluane ultramafic rocks are very close or identical to other igneous mafic and ultramafic intrusives in northern Stikinia, such as: (1) gabbro and pyroxenites (208 Ma) in the Lewes River arc/ Tally Ho Shear Zone of southern Yukon, (Tizzard et al, 2009) (2) intrusive and volcanic rocks in the Stuhini Group of northwestern BC (Mihalynuk,1999; Logan et al, 2012, 2013), (3) websterite, clinopyroxenite and hornblendite in the Hotailuh batholith (220 – 216 Ma – vanStraaten et al, 2012). The age, geochemical similarity and proximity of these rocks in these locales are striking (Fig. 12). If related, then the occurrence of plutonic ultramafic rock from late Triassic arcs of Stikinia within the Kluane Schist, a package dominated by pelitic sediments accumulating in a fore- or back arc setting (Israel et al, 2011), requires further explanation.

Although the Kluane ultramafic rocks have distinct geochemical traits of being from plutonic peridotite and pyroxenite protoliths, they cannot have been intrusive into the sedimentary protolith of the Kluane Schist. The detritus forming the Kluane schist is younger than 95 Ma (Israel et al, 2011; Stanley, 2012), and thus its deposition post-dates by ~ 100 m.y. the crystallization age of the ultramafic rocks at Doghead Point. The ultramafic bodies must be detritus, deposited into a mainly pelitic sedimentary host of the Kluane Schist prior to its deformation and metamorphism beginning at 82 Ma. Because the ultramafic bodies can be decimeter to kilometer in size, and interleaved on a variety of scales throughout the schist over a broad area, they were likely derived from a source

local to the basin in which they were deposited. The most obvious setting and mechanism for deposition of the ultramafic rocks is as foreign blocks or 'knockers' of plutonic rocks in an olistostrome (melange), likely in a fore-arc setting, similar to the metabasite and ultramafite 'knockers' that characterize the classic Franciscan of California (Cowan, 1978; Karig, 1980). Large blocks of arc-related plutonic rock is consistent with isotopic lines of evidence for juvenile arc detritus accumulating in a fore-arc setting for the protolith of the Kluane schist (Mezger et al, 2001b).

Deposition of the ultramafic intrusive rocks in a fore-arc as olistostromes also makes a cogent temporal and spatial connection between the Kluane Schist with accreted late Triassic arcs segments and related structures in the northern Cordillera. High strain shear zones from north to south, including the Takhini, Tally Ho, Llewellyn and Wann River, characterize the northwestern edge of Stikinia. The Takhini, Tally Ho, and Wann River were active between 208 and ~170 Ma, and eventually imbricated the west-facing late Triassic Lewes River - Stuhini arc within an east-verging thrust stack (Tizzard et al, 2009). The Llewellyn fault is a brittle-ductile dextral fault that was also active through late Triassic to Jurassic, but also reactivated to as late as Eocene (Mihalynuk and Rousse, 1988). These structures are within 100 km of the Kluane Schist (present coordinates). Arc parallel translation or arc-parallel thrusting along such structures exhumed peridotitic and pyroxenitic intrusive arc rocks of the deeper crust, making them available for eventual transport to a Kluane forearc basin forming as young as 95 m.y. ago.

If the Kluane pyroxenite and peridotite protoliths are sourced in the late Triassic Lewes River-Stuhini arc, this would also require an 80 m.y. year period of crustal stability and low erosion rates subsequent to their exhumation along Late Triassic to

Early Jurassic faults, and prior to their deposition into the forearc basin between 95 and 82 Ma, the age of deposition of the Kluane Schist (Fig. 12). Some late stage exhumation and transport along the more recently activated Llewelynn fault could explain a short distance of transport for large sized ultramafic blocks in the melange. The late dextral movement on the Llewellyn fault would also explain how a source for large blocks of Lewes River-Stuhini arc peridotite and pyroxenite are now located 10 – 200 km southeast of the Kluane basin. In this way, the Kluane fore arc basin would be west-facing, and bordered to the east perhaps by, and proximal to, a syn-depositional dextral strike slip fault or faults. Furthermore, incision of the Kluane fore-arc basin by this or related strike slip faults is a compelling mechanism for imbricating large knockers in the accretionary prism of a fore-arc (Karig, 1980).

Acknowledgements - We thank D. Hakonen of Trans North for our helicopter support to Doghead Point. Samples near Talbot Arm were collected by S.G. Shellnut. This research was supported by NSERC of Canada Discovery Grants and Yukon Geological Survey Grants to DC and STJ.

References

Alt, J.C., Honnorez, J., Laverne, C., and Emmermann, R. 1986. Hydrothermal alteration of a 1 Km section through the upper oceanic crust, Deep Sea Drilling Project Hole 504B: Mineralogy, chemistry, and evolution of seawater-basalt interactions. Journal of Geophysical Research, 91: 10,309-310,335.

Babechuk, M.G., Kamber, B.S., Greig, A., Canil, D. and Kodolanyi, J.N. 2010. The behaviour of tungsten during mantle melting revisited with implications for planetary differentiation time scales. Geochimica et Cosmochimica Acta, 74: 1448-1470.

Canil, D. 2004. Mildly incompatible elements in peridotites and the origins of mantle lithosphere: Lithos, 77: 375-393.

Canil, D., Johnston, S.T., and Mihalynuk, M. 2006. Mantle redox in Cordilleran ophiolites as a record of oxygen fugacity during partial melting and the lifetime of mantle lithosphere. Earth and Planetary Science Letters, 248: 91-102.

Canil, D. and Lee, C.T.A. 2009. Were deep cratonic mantle roots hydrated in Archean oceans? Geology, 37: 667-670.

Canil, D., Crockford, P.W., Rossin, R., Telmer, K. Mercury abundances in the crust and mantle and relevance to the moderately volatile element budget of the Earth, Chemical Geology, submitted May 2014.

Coleman, R.G. and Keith, T. 1971. A chemical study of serpentinization—Burro Mountain, California, Journal of Petrology 12: 311-328.

Cowan, D.S. 1978. Origin of blueschist-bearing chaotic rocks in the Franciscan Complex, San Simeon, California, Geological Society of America Bulletin 89: 1415-1423

DeBari, S. M. and Coleman, R. G. 1989. Examination of the deep levels of an island arc: evidence from the Tonsina ultramafic-mafic assemblage, Tonsina, Alaska, Journal of Geophysical Research, v. 94, p. 4373-4391.

Den Tex, E., 1969. Origin of ultramafic rocks, their tectonic setting and history: A contribution to the discussion of the paper" The origin of ultramafic and ultrabasic rocks" by P.J. Wyllie. Tectonophysics, 7: 457-488.

Doriguetto, A. C., Fernandes, N. G. Persiano, A. I. C., Nunes Filho, E. Grene`che, J. M., Fabris, J. D. 2003. Characterization of a natural magnetite. Physics and Chemistry of Minerals, 30: 249 – 255

Evans, B.W. 1977. Metamorphism of alpine peridotite and serpentinite. Annual Review of Earth and Planetary Sciences, 5: 397.

Erdmer, P. and Mortensen, J. K. 1993. A 1200-Km-Long Eocene Metamorphic-Plutonic Belt in the Northwestern Cordillera - Evidence from Southwest Yukon. Geology 21: 1039-1042.

Fecova, K. 2009. Conuma River and Leagh Creek intrusive complexes: windows into mid- crustal levels of the Jurassic Bonanza Arc, Vancouver Island, British Columbia. MSc thesis, Simon Fraser University, 221 pp.

Frost, B.R. 1975. Contact metamorphism of serpentinite, chloritic blackwall and rodingite at Paddy-Go-Easy Pass, Central Cascades, Washington, Journal of Petrology 16: 272-313. doi: 10.1093/petrology/16.1.272

Gabrielse, H. 1991. Late Palezoic and Mesozoic terrane interactions in north-central British Columbia. Canadian Journal of Earth Sciences 28: 947-957.

Gillis, K.M., and Banerjee, N.R. 2000. Hydrothermal alteration patterns in supra-subduction zone ophiolites. In Ophiolites and Oceanic Crust: New Insights from Field Studies and Ocean Drilling Program. Edited by Y. Dilek, E. Moores, D. Elthon, A. Nicolas, Geological Society of America Special Paper 349, Geological Society of America Boulder, CO. pp. 283-297.

Greene, A. R., DeBari, S. M., Kelemen, P., Blusztajn, J., and Clift, P. D. 2006. A detailed geochemical study of island arc crust: the Talkeetna arc section, South-Central Alaska, Journal of Petrology, 47: 1051-1093.

Gruau, G., Bernard-Griffiths, J. and Lecuyer, C. 1998. The origin of U-shaped rare earth patterns in ophiolite peridotites: Assessing the role of secondary alteration and melt/rock reaction. Geochimica et Cosmochimica Acta, 62: 3545-3560.

Gruau, G., Lecuyer, C., Bernard-Griffiths, J. and Morin, N. 1991. Origin and petrogenesis of the Trinity Ophiolite Complex (California): new constraints from REE and Nd isotope data. In: M.A. Menzies, C. Dupuy and A. Nicolas (Editors), Orogenic lherzolites and mantle processes. Oxford University Press,

Heaman, L. M., Erdmer, P. E. and Owen, J. V. 2002. U-Pb geochronologic constraints on the crustal evolution of the Long Range Inlier, Newfoundland. Canadian Journal of Earth Sciences, 39: 845-865

Israel, S., Murphy, D., Bennett, V., Mortensen, J. and Crowley, J. 2011. New insights into the geology and mineral potential of the Coast Belt in southwestern Yukon. In: Yukon Exploration and Geology 2010, K.E. MacFarlane, L.H. Weston and C. Relf (eds.), Yukon Geological Survey, p. 101-123.

Jaffey, A.H., Flynn, K.F., Glendenin, L.E., Bentley, W.C., Essling, A.M.,1971. Precision measurement of half-lives and specific activities of 235U and 238U. Physics Review C4: 1889–1906.

Jagoutz, E., Palme, H., Baddenhausen, H., Blum, K., Cendales, M., Dreibus, G., Spettel, B., Lorenz, V., and Wanke, H. 1979. The abundances of major, minor and trace elements in the earth's mantle as derived from primitive ultramafic nodules, in 10th Lunar and Planetary Science Conference, p. 2031-2050.

Jagoutz, O., Muntener, O., Ulmer, T., Burg, J.P., Dawood, H., Hussain, S. 2007. Petrology and mineral chemistry of lower crustal intrusions: the Chilas Complex, Kohistan (NW Pakistan), Journal of Petrology 48: 1895-1953.

Jenner, G.A. 1996. Trace element geochemistry of igneous rocks: geochemical nomenclature and analytical geochemistry; in Trace Element Geochemistry of Volcanic Rocks: Applications for Massive Sulfide Exploration, D.A.Wyman (ed.), Geological Association of Canada, Short Course Notes, v. 12, p. 51–77.

Johnston, S.T. 2008. The Cordilleran ribbon continent of North America, Annual Reviews of Earth and Planetary Sciences, 36:495–530.

Johnston, S.T. and Erdmer, P. 1995. Hot-side-up aureole in southwestern Yukon and limits on terrane assembly of the northern Canadian Cordillera. Geology, 23: 419-422.

Johnston, S.T., and Canil, D. 2007. The crustal architecture of SW Yukon, northern Cordillera: Implications for crustal growth in a convergent margin orogen, Tectonics, TC1006, doi:10.1029/2006TC001950

Karig, D.E. 1980. Material transport within accretionary prisms and the ‘knocker’ problem. Journal of Geology, 88: 27-39.

Larocque, J., and Canil, D. 2010. The role of amphibole in the evolution of arc magmas and crust: the case from the Jurassic Bonanza arc section, Vancouver Island, Canada. Contributions to Mineralogy and Petrology, 159: 475-492.

Lee, C.A., Leeman, W.P., Canil, D., and Li, Z.A. 2005. Similar V/Sc systematics of MORB and arc basalts: implications for the oxygen fugacities of their mantle source regions. Journal of Petrology, 46: 2313-2336.

Le Roux, V., Bodinier, J. L., Tommasi, A., O. Alard, O., Dautria, J. M., Vauchez, A., and Riches, A. J. V. 2007. The Lherz spinel lherzolite: Refertilized rather than pristine mantle. Earth and Planetary Science Letters, 259: 599–612 DOI: 10.1016/j.epsl.2007.05.026

Liou, J.G., Kuniyoshi, S., and Ito, K. 1974. Experimental studies of the phase relations between greenschist and amphibolites in a basaltic system. American Journal of Science, 274: 613-632.

Liang, Y., and Elthon, D. 1990. Evidence from chromium abundances in mantle rocks for extraction of picrite and komatiite melts, Nature 343: 551 – 553

Logan, J.M. and Iverson, O. 2013. Dease Lake Geoscience Project: geochemical characteristics of Tsaybahe, Stuhini and Hazelton volcanic rocks, northwestern British Columbia (NTS 104I, J); in Geoscience BC Summary of Activities 2012, Geoscience BC, Report 2013-1, p. 11–32.

Logan, J.M., Diakow, L.J., van Straaten, B.I., Moynihan, D.P., Iverson, O. 2012. QUEST-Northwest mapping: BC Geological Survey Dease Lake Geoscience Project, northern British Columbia (NTS 104I, J); in Geoscience BC Summary of Activities 2011, Geoscience BC, Report 2012-1, p. 5–14.

Massone, H.J. 1985. The upper thermal stability of chlorite + quartz: an experimental study in the system MgO-Al2O3-SiO2-H2O, Journal of Metamorphic Geology, 7: 567–581,

McDonough, W.F. and Sun, S.S. 1995. The composition of the earth. Chemical Geology 120: 223-253.

Mezger, J.E. 2000. 'Alpine-type' ultramafic rocks of the Kluane metamorphic assemblage, southwest Yukon: Oceanic crust fragments of a late Mesozoic back-arc basin along the northern Coast Belt. In: Yukon Exploration and Geology 1999, D.S. Emond and L.H. Weston (eds.), Exploration and Geological Services Division, Yukon, Indian and Northern Affairs Canada, 127-138.

Mezger, J. E. 2003. Geology of the Dezadeash Range and adjacent northern Coast Mountains (115A), southwestern Yukon: Re-examination of a terrane boundary. Yukon Exploration and Geology 2002. D. S. Emond and L. L. Lewis. Whitehorse, YT, Exploration and Geological Services Division, Yukon Region, Indian and Northern Affairs Canada: 149-163.

Mezger, J. E., Chacko, T. and Erdmer, P. 2001a. Metamorphism at a late Mesozoic accretionary margin: a study from the Coast Belt of the North American Cordillera. Journal of Metamorphic Geology 19: 121-137.

Mezger, J. E., Creaser, R. A. Erdmer, P., and Johnston, S.T. 2001b. A Cretaceous back-arc basin in the Coast Belt of the northern Canadian Cordillera: evidence from geochemical and neodymium isotope characteristics of the Kluane metamorphic assemblage, southwest Yukon." Canadian Journal Earth Sciences 38: 91-103.

Mihalynuk, M. G. and Rouse, J. N. 1988. Preliminary Geology of the Tutshi Lake Area, Northwestern British Columbia (104M/15), Geological Fieldwork 1987: A Summary of Field Activities and Current Research, Paper 1988. Province of British Columbia, Ministry of Energy, Mines and Petroleum Resources, Mineral Resources Division, Geological Survey Branch, Victoria BC, 217–232.

Mihalynuk , M.G. 1999. Geology and mineral resources of the Tagish Lake area (NTS 104M/8, 9, 10E, 15 and 104N/12W), northwestern British Columbia, Geologicla Survey Britihsh Columbia, Bulletin 105.

Mortensen, J.K., Ghosh, D.K. and Ferri, F. 1995. U-Pb geochronology of intrusive rocks associated with copper-gold porphyry deposits in the Canadian Cordillera. In: Porphyry deposits of the Northwestern Cordillera of North America, Canadian Institute of Mining and Metalurgy Special Volume 46

Münker, C., Wömer, G., Yogodzinski, G. and Churikova, T. 2004. Behaviour of high field strength elements in subduction zones: constraints from Kamchatka-Aleutian arc lavas; Earth and Planetary Science Letters, 224: 275– 293.

Palme, H., O'Neill, H.St.C. 2003. Cosmochemical estimates of mantle composition. pp. 1-38. In: The Mantle and Core (ed. R.W. Carlson) vol. 2 Treatise on Geochemistry (eds. H.D Holland and K.K. Turekian), Elsevier –Pergamon, Oxford.

Pawley, A. 1998. The reaction talc + forsterite = enstatite + H2O: New experimental results andpetrological implications. American Mineralogist, 83: 51-57.

Pearce, J.A. and Cann, J.R. 1973. Tectonic setting of basic volcanic rocks determined using trace element analyses; Earth and Planetary Science Letters, 19: 290–300.

Pearson, D.G., Canil, D., and Shirey, S.B. 2003. Xenoliths and Diamonds in Volcanic Rocks, in Treatise in Geochemistry, 3, Holland and Turekian (eds.) Elsevier Publishing, Amsterdam.

Snow, J.E. and Dick, H.J.B. 1995. Pervasive magnesium loss by marine weathering of peridotite. Geochimica et Cosmochimica Acta, 59: 4219-4235.

Stanley, B. 2012. Structural geology and geochronology of the Kluane Schist, southwestern Yukon Territory, MSc Thesis, University of Waterloo, 112 pp.

Tempelman-Kluit, D. 1974. Reconaissance geology of Aishihik Lake, Snag and part of Stewart River map-areas, west-central Yukon (115A, 115F, 115G and 115K). Geological Survey of Canada, Paper 73-41, 97 p.

Tizzard, A. M., Johnston, S. T., and Heaman, L. M. 2009. Arc imbrication during thick-skinned collision within the northern Cordilleran accretionary orogen, Yukon, Canada. Geological Society, London, Special Publications 318: 309-327

Trommsdorff, V., and Evans, B.W. 1972. Progressive metamorphism of antigorite schist in the Bergell tonalite aureole (Italy). American Journal of Science, 272: 423–437.

Trommsdorff, V., Lopez Sanchez-Vizcaino, V., Gomez-Pugnaire, M. T., and Müntener, O. 1998. High-pressure breakdown of antigorite to spinifex-textured olivine and orthopyroxene, S.E. Spain. Contributions to Mineralogy and Petrology, 132: 139–148.

van Straaten, B.J., Logan, J., and Diakow, L.J. 2012. Mesozoic magmatism and metallogeny of the Hotailuh batholith, northwestern British Columbia, Ministry of Energy, Mines and Natural Gas, British Columbia Geological Survey, Open File report 2012-10, 77 pp.

Figure Captions

Figure 1 - Regional geology of the western Canada showing allochtonous assemblages of the northern Cordillera (after Johnston and Canil, 2007). Dashed box shows location of Figure 2.

Figure 2 - Geology of southwest Yukon showing units of the crustal section described in text from east- to west (after Johnston and Canil, 2007). Dashed box shows location of Figure 3.

Figure 3 –Local geology of the Doghead Point area showing exposed ultramafic rocks (black) and an aeromagnetic anomaly defining their inferred extent in the subsurface (Mezger et al, 2000). Locations are given for samples in this study prefixed as either 'DC' or 'GS' (Table 1).

Figure 4 – Outcrops at Doghead Point ultramafic body. Red jacknife is 10 cm long for scale. (a) Meter sized layer of boudined light green chlorite-amphibole schist (CAS) interfoliated with dun brown antigorite-talc-olivine schist (ASO) (b) Crenulation cleavage in antigorite-talc-olivine schist. Pen magnet is 15 cm long for scale. (c) Large cm-sized porphyroblasts of olivine in talc schist. (d) Large cm-sized porphyroblasts of amphibole in the chlorite schist unit shown in (a). Pen top is 3 cm for scale. (e,f) Sawn rock slabs showing the scale of interfoliation between chlorite schist (darker layers) and talc schists (lighter layers). Scale bars are 2 cm.

Figure 5 – Photomicrographs of samples from Doghead Point in cross polarized light. (a) Olivine and talc overgowing antigorite in antigorite-talc-olivine schist. Note overgrowth of olivine on both generations of cleavage. Field of view is 35 mm. (b) Close up view of (a) with field of view of 2 mm. (c) Euhedral amphibole

porphyroblasts overgrown on chlorite matrix in chlorite schist. Field of view is 2 mm. (d) Granoblastic olivine and orthopyroxene in samples at the margin with the Ruby Range batholith. Small veinlets of late serpentine crosscut olivine. Field of view is 4mm.

Figure 6 – Covariation of Mg, Al and Si in ophiolite and orogenic massif peridotites residual from partial melt extraction (data sources compiled in Canil and Lee (2009). These samples plot along a depletion-refertilization trend from 'primitive mantle' (PUM – after McDonough and Sun, 1995) to olivine (OL). Also shown are a range of compositions for typical mantle orthopyroxene (OPX) and clinopyroxene (CPX) from spinel peridotites (adopted from Pearson et al, 2003). The Kluane ultramafic rocks, defined as having Mg/Mg+Fe > 0.9 (Table 1), plot mostly along a flat slope, displaced from the residue-refertilization trend of mantle peridotites toward pyroxene-rich components.

Figure 7 – Covariation of MgO with Cu, S, Sc and V in ophiolite and orogenic massif peridotites compared with those for Kluane ultramafic rocks. Data for Sc and V were compiled in Canil and Lee (2009), whereas those for Cu and S are from Canil et al (submitted).

Figure 8 - Covariation of Sc as a depletion index with V and Cr in peridotites from Cordilleran mantle ophiolites (Canil et al, 2006; Babechuk et al, 2010) compared with those for Kluane ultramafic rocks (this study) and igneous cumulate peridotites from the GEOROC database (http://georoc.mpch-mainz.gwdg.de/georoc/). Note the displacement of the trend for Kluane ultramafic rocks and cumulate peridotites from the mantle residues.

Figure 9 – Primitive mantle normalized trace element patterns for Kluane ultramafic rocks (open circles – antigorite-talc-olivine schists) and mafic rocks (open triangles – chlorite-amphibole schists) compared to (a) Cordilleran ophiolite peridotites (data sources as in Fig 7) and (b) pyroxenites, basalt and gabbros from late Triassic arcs in Stikinia of the northern Cordillera. Data for pyroxenites from the Tally Ho Shear Zone (Lewes River arc) from Tizzard et al (2009). Those from Stuhini arc from Logan et al (2012). Note the similarity of the Kluane samples to the late Triassic arc rocks.

Figure 10 – U-Pb concordia diagram for three zircon fractions in sample GS01-012 from near Talbot Arm (see Figure 3). Error ellipses plotted at 95% confidence. One zircon fraction plots near concordia and when regressed with one of the two other highly discordant fractions produces a lower intercept age of ~ 201 Ma.

Figure 11 – Covariation of molar Si+Al with Mg+Fe (black closed symbols) and Ca+Na (red open symbols) in the Kluane mafic (diamonds) and ultramafic (circles) rocks. Also shown for illustrative purposes are amphibole-peridotite and -pyroxenite cumulates from the Jurassic Bonanza arc (Larocque and Canil, 2010; Fecova, 2010). The molar plot shows the mineral stoichiometric control on rock compositions. Note the trend of the Kluane mafic rocks (diamonds) along control lines of olivine, hornblende and/or pyroxene accumulation.

Figure 12 – Summary of ages for intrusions (filled bars) and movement on major fault zones (open bars) in southwest Yukon and northwestern BC. Note the overlap in age of Kluane ultramafic rocks with arc related mafic/ultramafic intrusives in northern Stikinia. Movement on the Llewellyn Fault extends to the youngest U-Pb detrital

zircon age in the Kluane Schist. Data sources are: Kluane ultramafic rocks - this study; Tally Ho Shear Zone– Tizzard et al (2008); Kluane Schist - Israel et al, (2011); Stanley, (2012); Hotuilah batholith and Stuhini arc - van Straaten et al, (2012); Logan et al (2012).

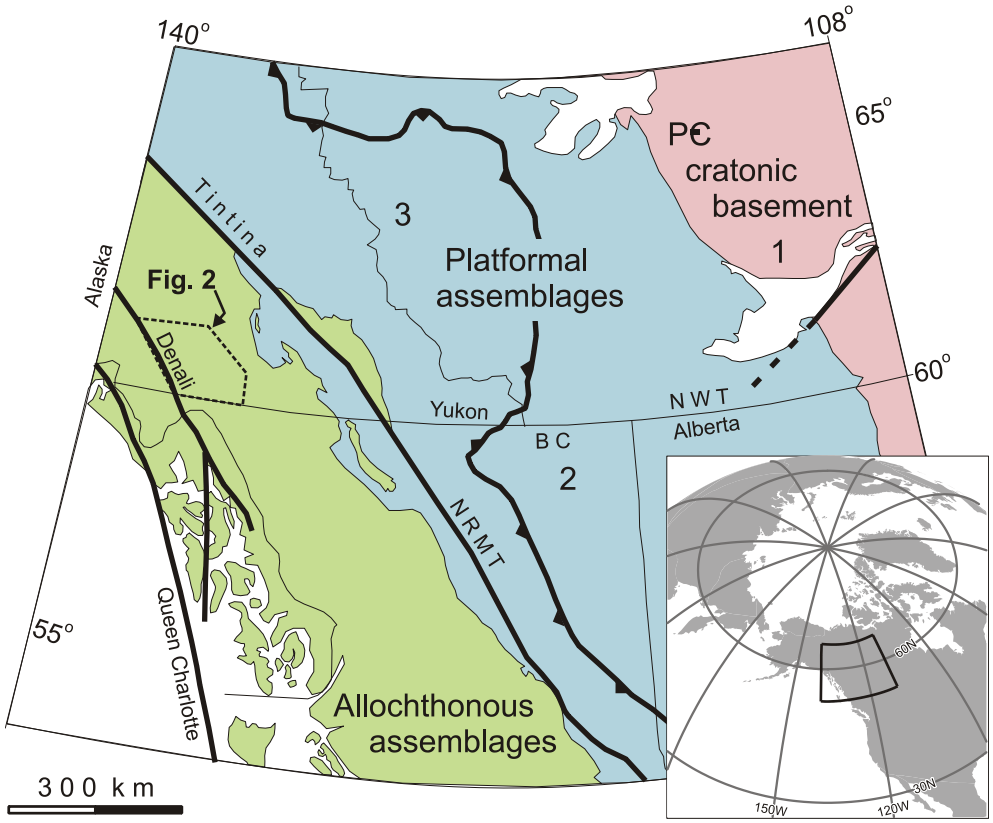
140°
108°
65°
60°
55°
PЄ
cratonic
basement
1
3
Platformal
assemblages
Tintina
Alaska
Fig. 2
Denali
Yukon
N W T
Alberta
B C
2
NRMT
Queen Charlotte
Allochthonous
assemblages
3 0 0 k m
60N
30N
150W
120W

Fig 1

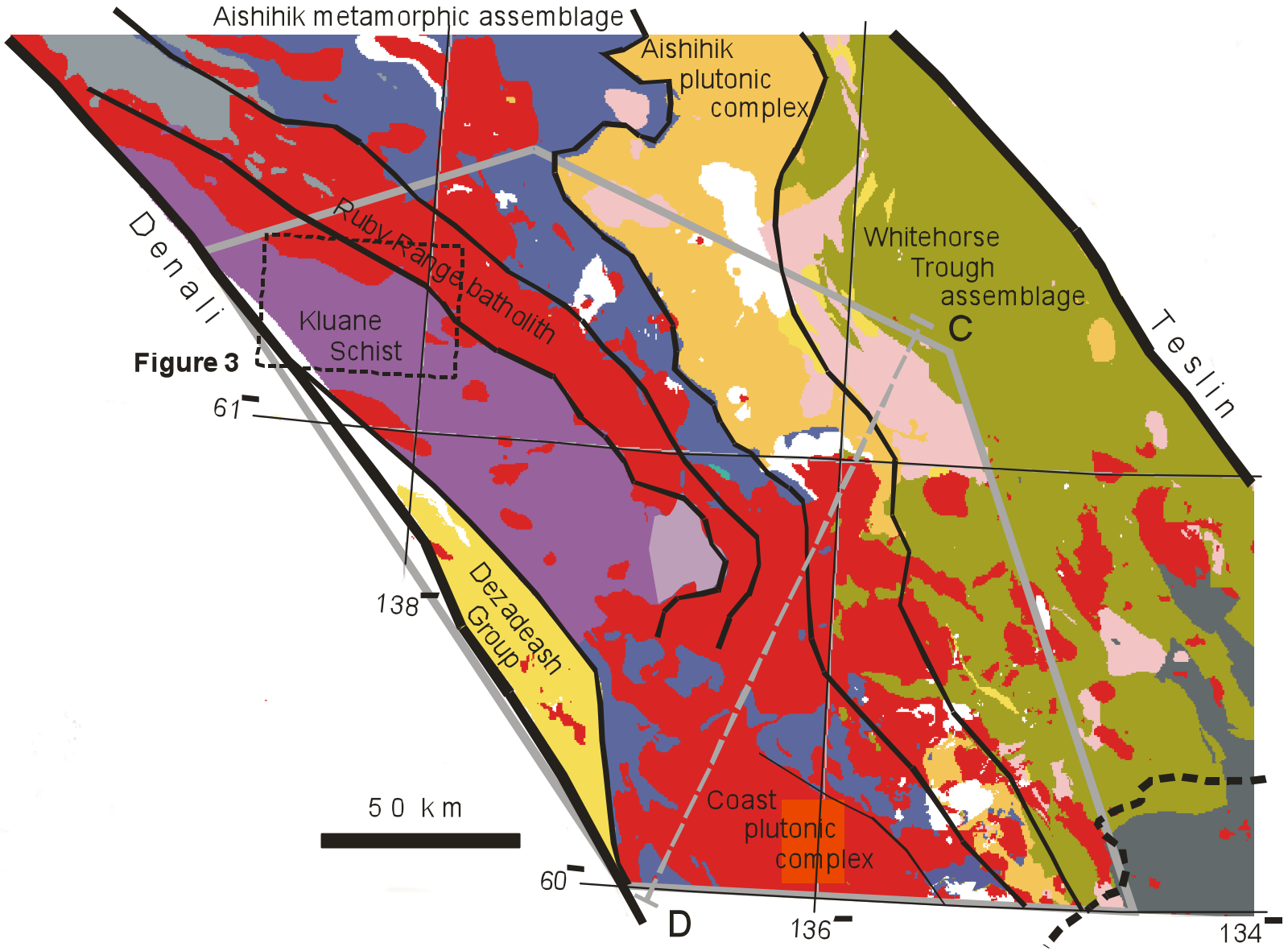
Aishihik metamorphic assemblage
Aishihik plutonic complex
Ruby Range batholith
Kluane Schist
Denali
Whitehorse Trough assemblage
C
Teslin
Figure 3
61
138
Dezadeash Group
50 km
Coast plutonic complex
60
D
136
134

Fig 2

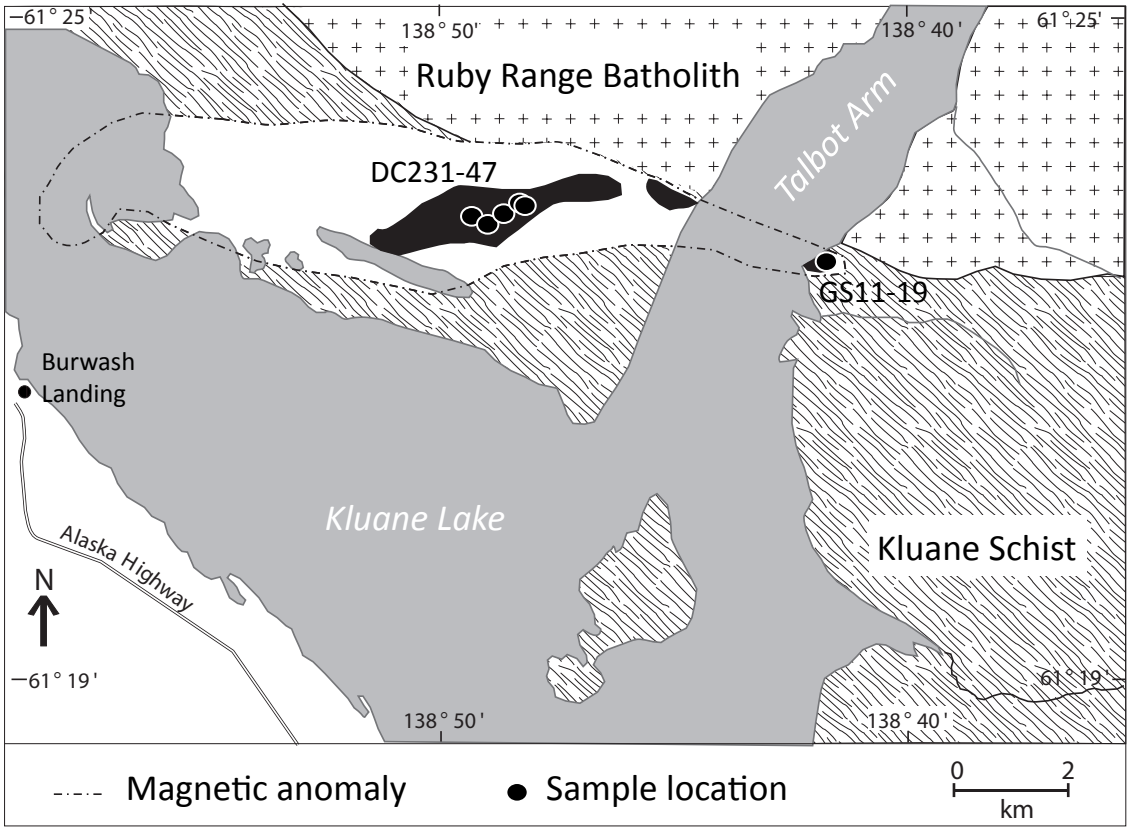
61° 25'
138° 50'
138° 40'
61° 25'
Ruby Range Batholith
Talbot Arm
DC231-47
GS11-19
Burwash
Landing
Kluane Lake
Kluane Schist
Alaska Highway
N
61° 19'
138° 50'
138° 40'
61° 19'
Magnetic anomaly
Sample location
0
2
km

Fig 3

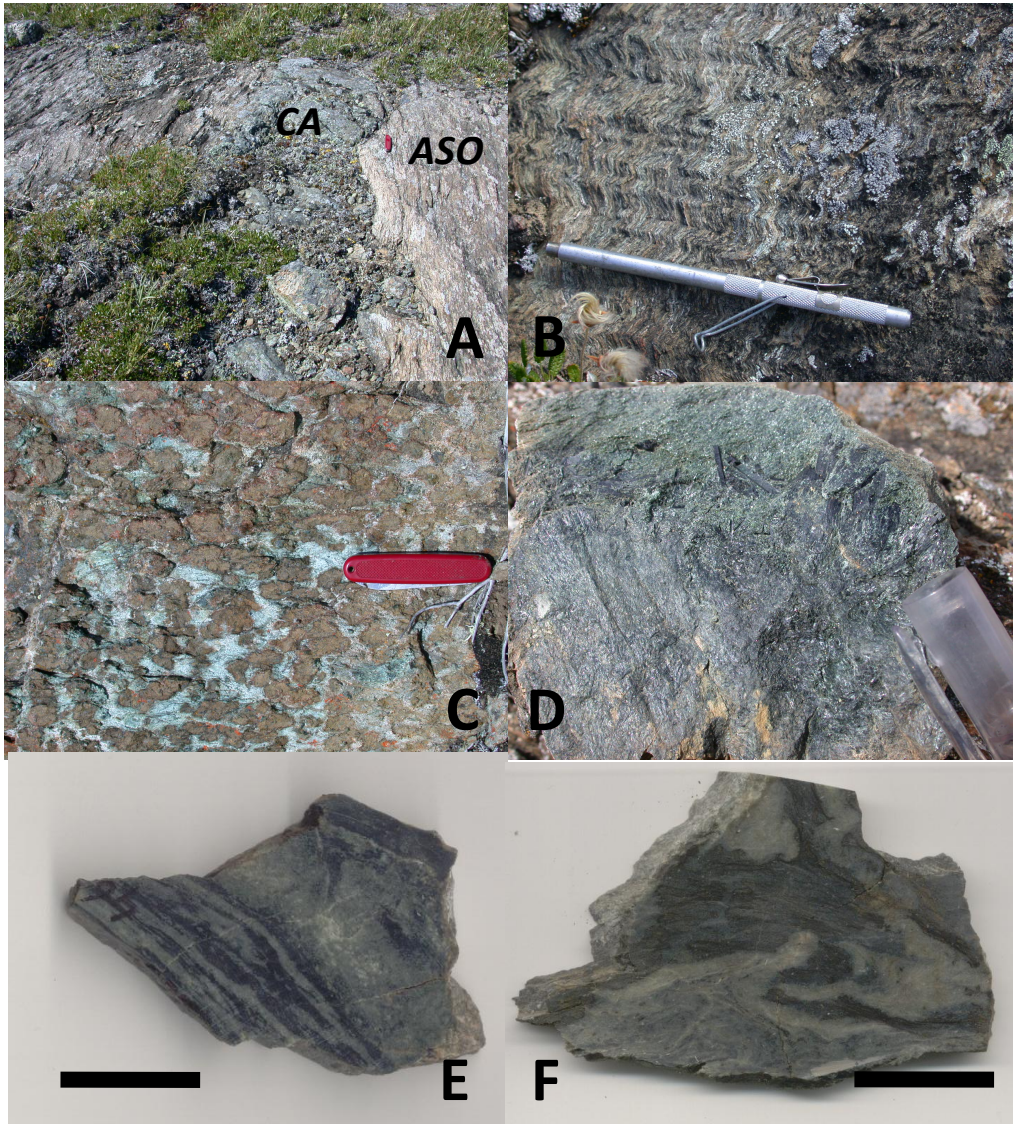

Fig 4

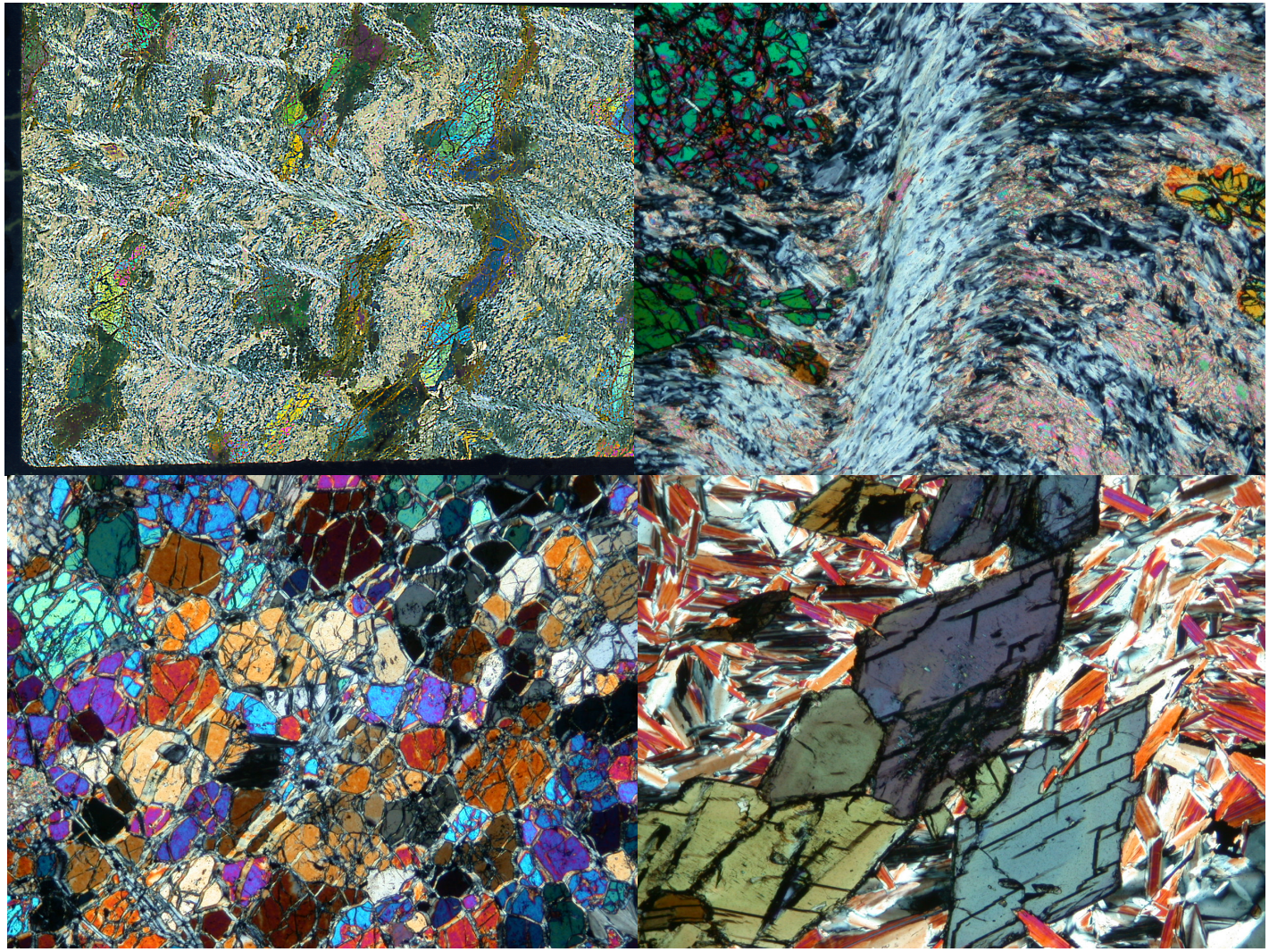

Fig 5

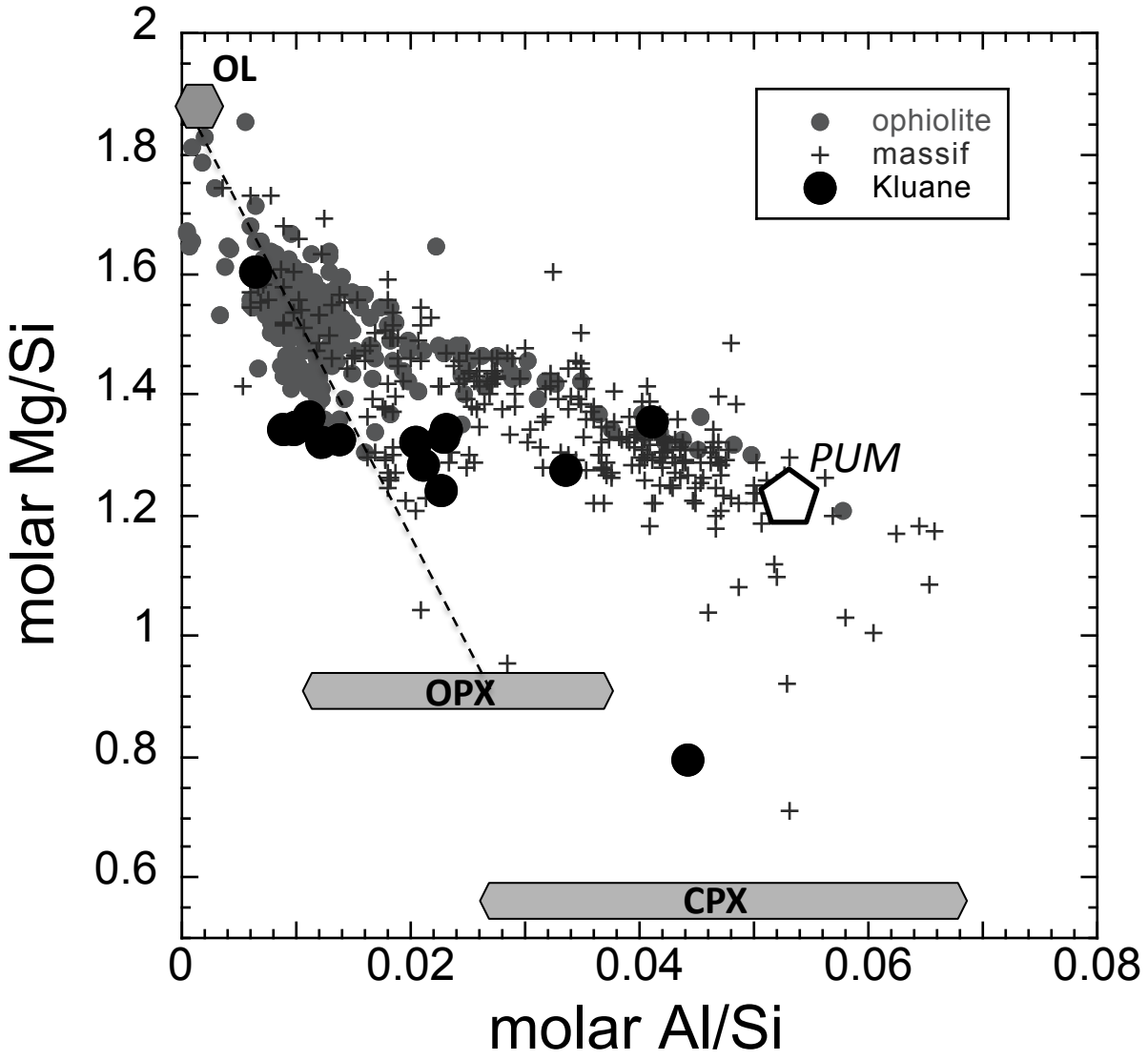
OL
ophiolite
massif
Kluane
PUM
OPX
CPX
molar Mg/Si
molar Al/Si
2
1.8
1.6
1.4
1.2
1
0.8
0.6
0
0.02
0.04
0.06
0.08

Fig 6

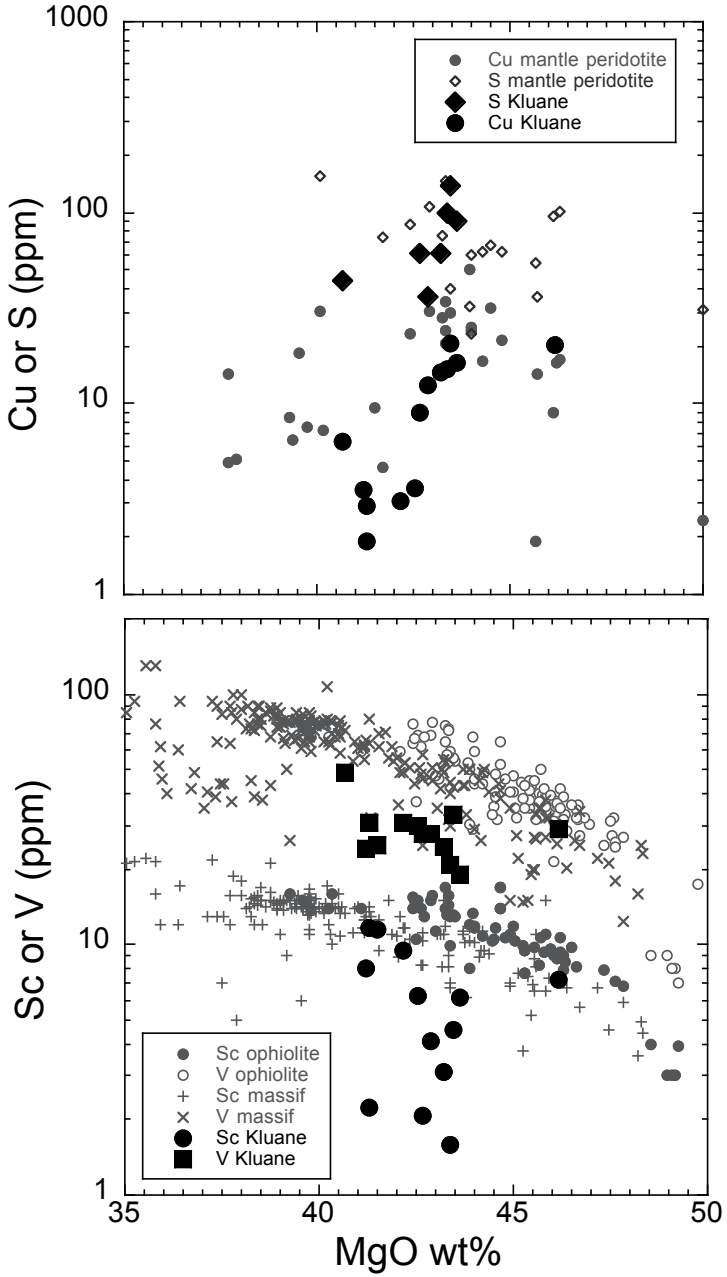
1000
100
10
1
Cu or S (ppm)
Cu mantle peridotite
S mantle peridotite
S Kluane
Cu Kluane
100
10
1
Sc or V (ppm)
Sc ophiolite
V ophiolite
Sc massif
V massif
Sc Kluane
V Kluane
35
40
45
50
MgO wt%

Fig 7

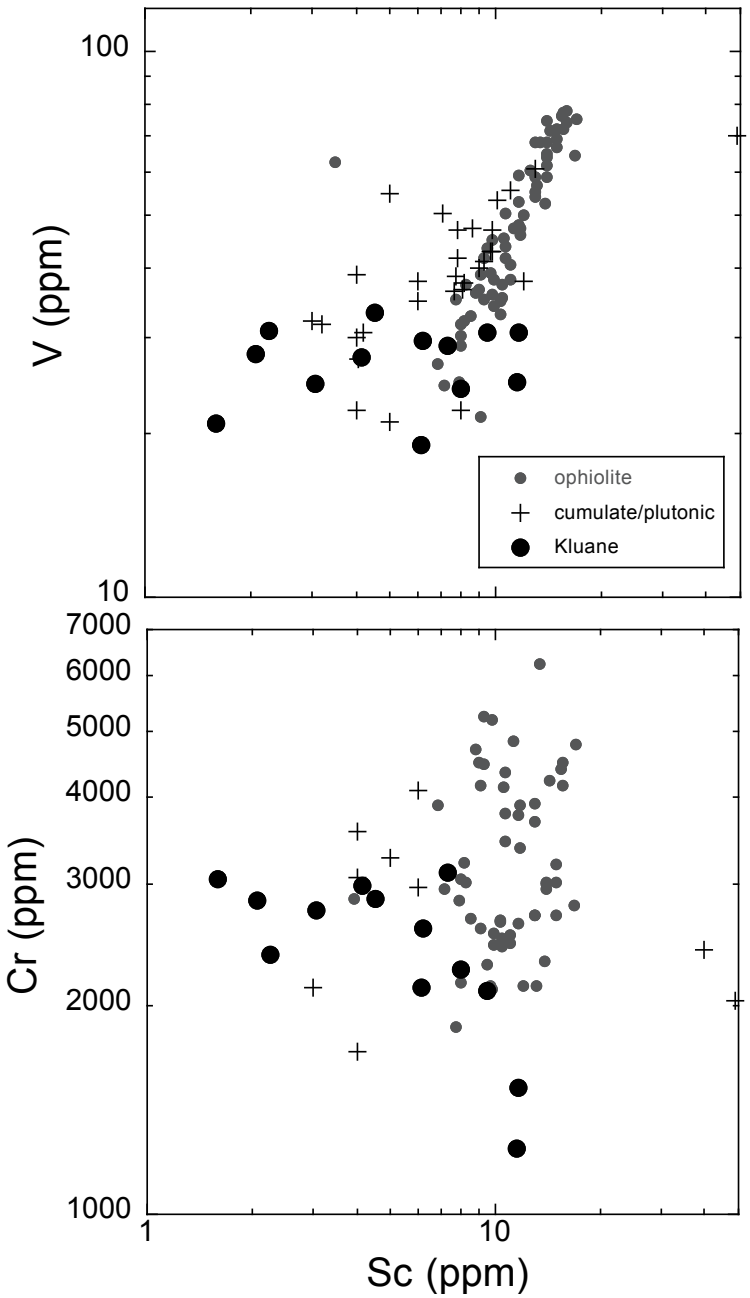
100
10
V (ppm)
ophiolite
cumulate/plutonic
Kluane
7000
6000
5000
4000
3000
2000
1000
Cr (ppm)
1
10
Sc (ppm)

Fig 8

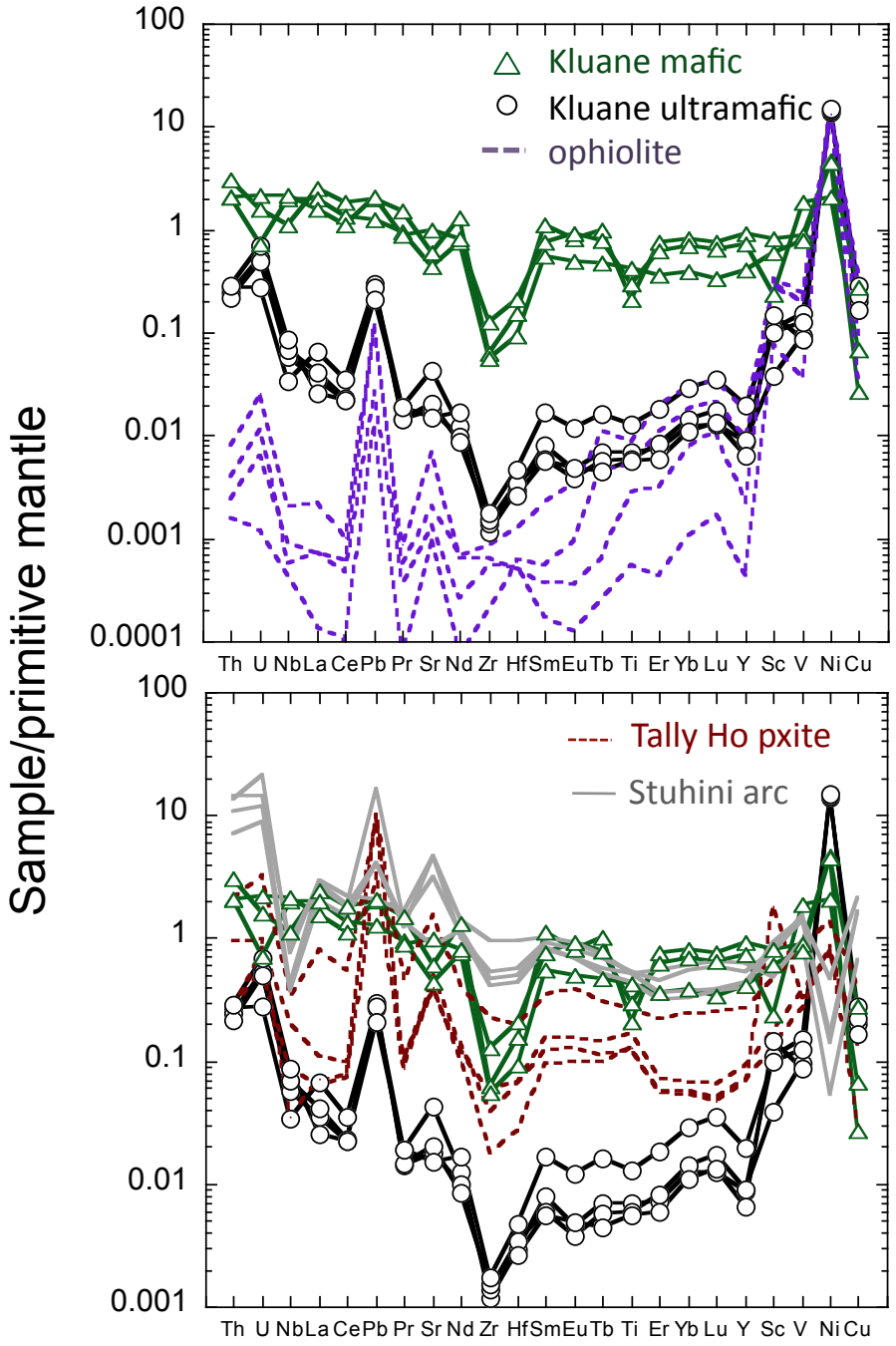
Sample/primitive mantle
100
10
1
0.1
0.01
0.001
0.0001
Kluane mafic
Kluane ultramafic
ophiolite
Th U Nb La Ce Pb Pr Sr Nd Zr Hf Sm Eu Tb Ti Er Yb Lu Y Sc V Ni Cu
100
10
1
0.1
0.01
0.001
Tally Ho pxite
Stuhini arc
Th U Nb La Ce Pb Pr Sr Nd Zr Hf Sm Eu Tb Ti Er Yb Lu Y Sc V Ni Cu

Fig 9

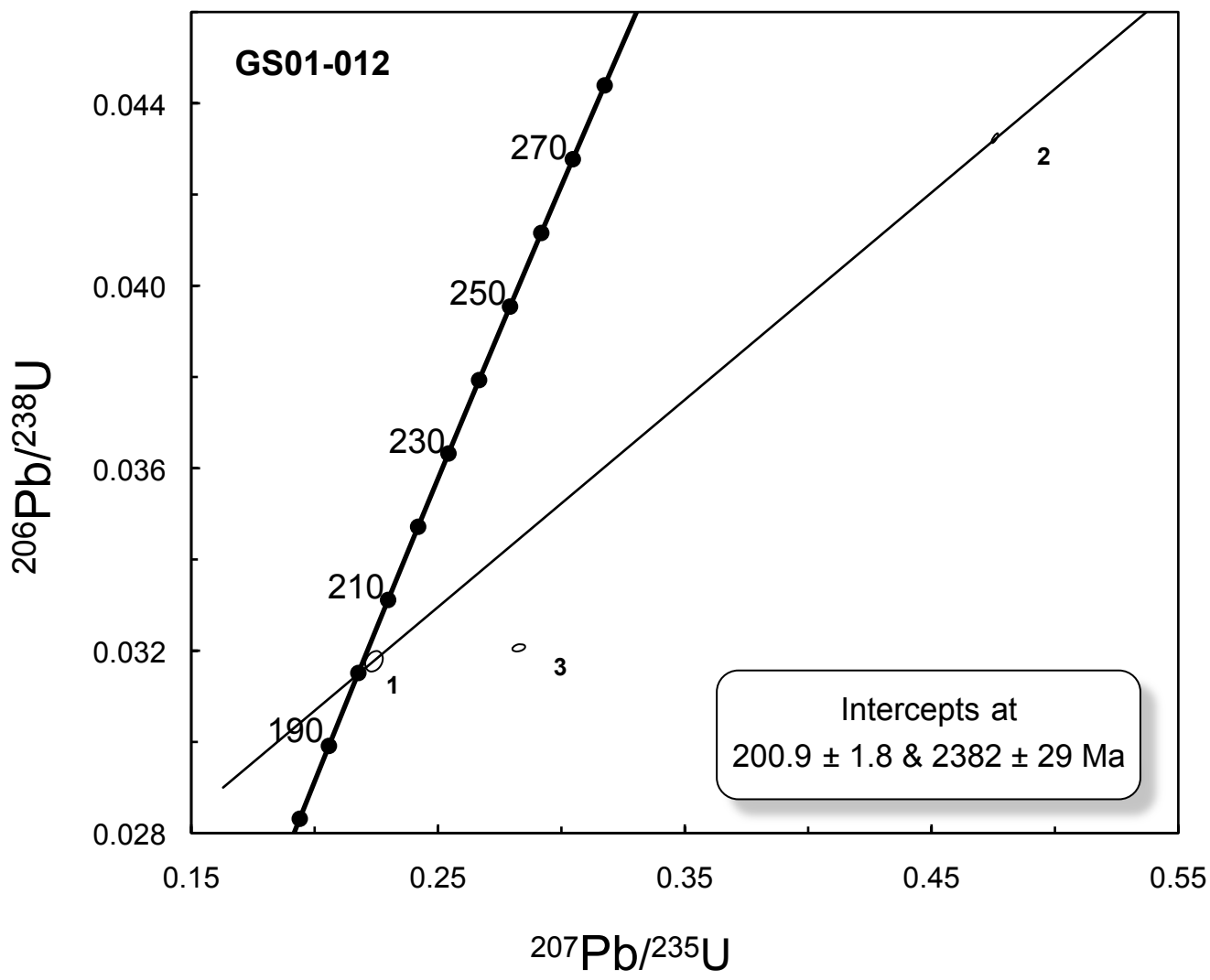
GS01-012
0.044
0.040
0.036
0.032
0.028
270
250
230
210
190
1
2
3
Intercepts at
200.9 ± 1.8 & 2382 ± 29 Ma
0.15
0.25
0.35
0.45
0.55
206Pb/238U
207Pb/235U

Fig 10

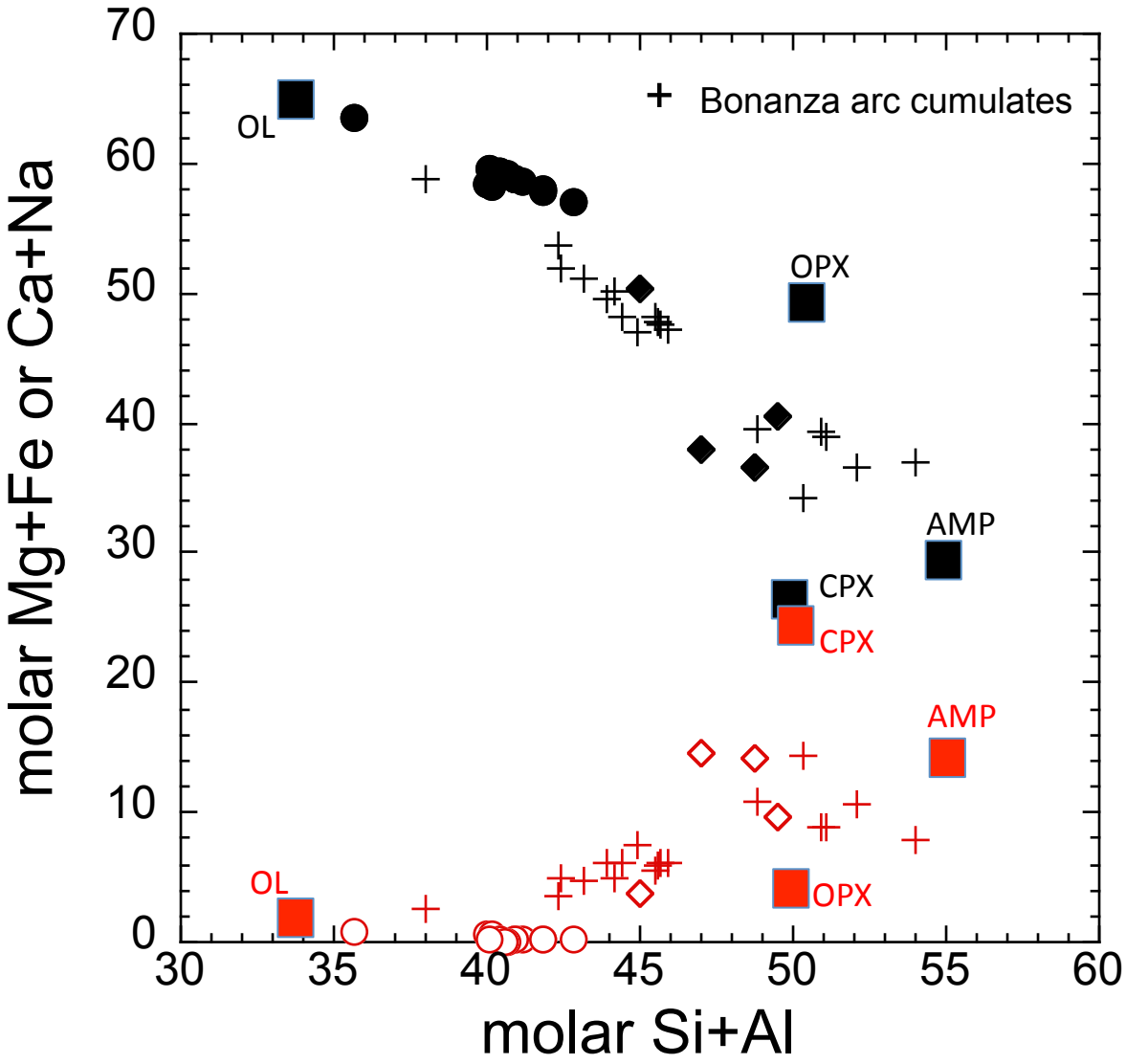
Bonanza arc cumulates
OL
OPX
AMP
CPX
CPX
AMP
OL
OPX
molar Mg+Fe or Ca+Na
molar Si+Al
70
60
50
40
30
20
10
0
30
35
40
45
50
55
60

Fig 11

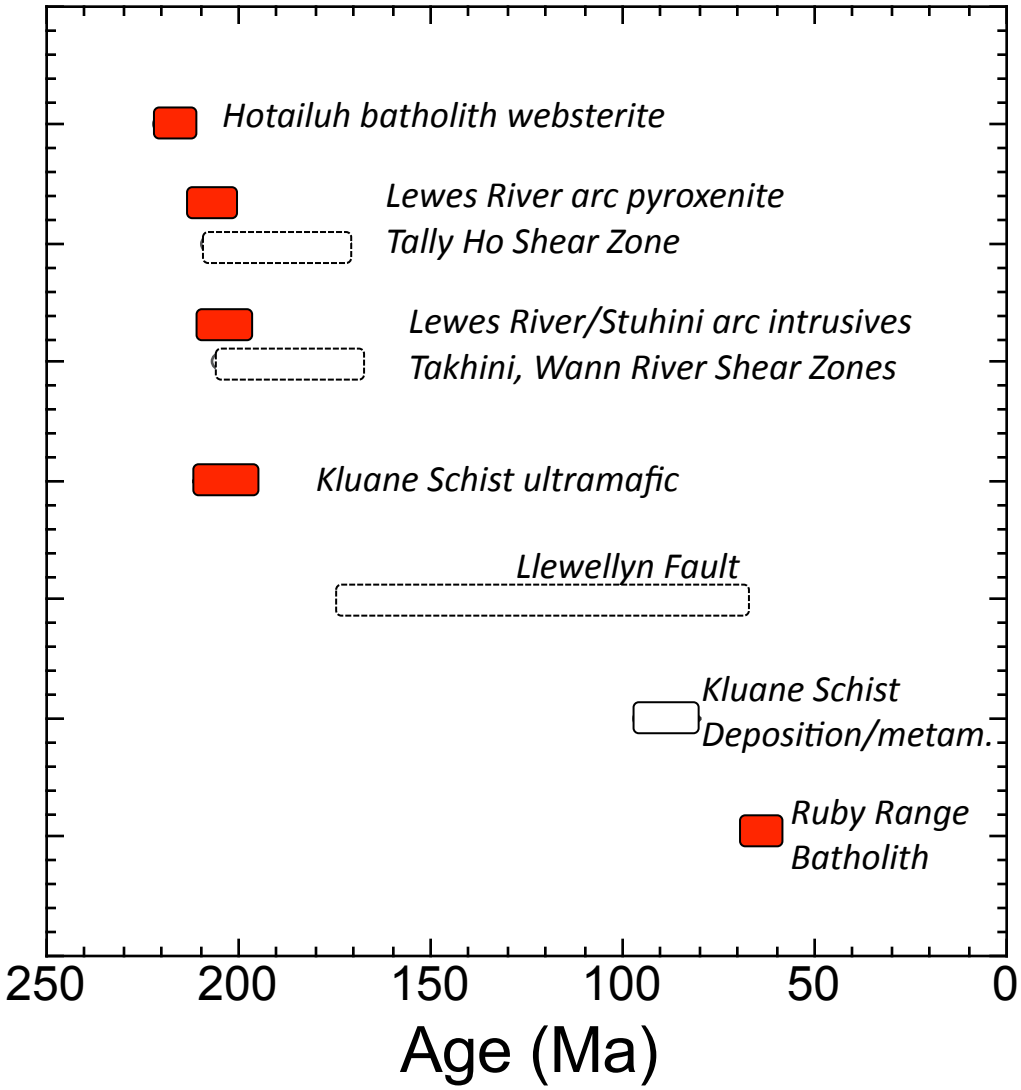
Hotailuh batholith websterite
Lewes River arc pyroxenite
Tally Ho Shear Zone
Lewes River/Stuhini arc intrusives
Takhini, Wann River Shear Zones
Kluane Schist ultramafic
Llewellyn Fault
Kluane Schist
Deposition/metam.
Ruby Range
Batholith
250
200
150
100
50
0
Age (Ma)

Fig 12

Table 1- Mineral chemistry in selected rocks from Doghead Point

Sample	Na2O	MgO	Al2O3	SiO2	K2O	CaO	TiO2	Cr2O3	MnO	FeO	NiO	TOTAL	Oxygens	Na+	Mg2+	Al3+	Si4+	K+	Ca2+	Ti4+	V3+	Cr3+	Mn2+	Fe2+	Ni2+	CATIONs	Mg/(Mg+Fe)
Chlorite-Amphibole Schists																											
DC0235 Amp pblast	1.68	17.9	6.61	48.0	0.22	12.29	0.26	0.07	0.16	8.02	-	95.41	23	0.478	3.921	1.148	7.045	0.041	1.933	0.029	0.000	0.008	0.020	0.987	0.000	15.608	0.799
DC0235 Amp relic	2.63	13.9	12.26	41.8	0.41	11.99	0.42	0.07	0.16	12.33	-	96.01	23	0.766	3.109	2.176	6.295	0.080	1.934	0.048	0.000	0.008	0.020	1.553	0.000	15.988	0.667
DC0235 Cpx relic	0.75	14.1	1.09	53.0	0.02	23.20	0.04	0.07	0.16	6.13	-	98.59	6	0.055	0.788	0.048	1.988	0.001	0.933	0.001	0.000	0.002	0.005	0.192	0.000	4.014	0.804
DC0235 Chl	0.01	27.3	19.24	29.9	0.01	0.01	0.05	0.09	0.14	9.56	-	86.32	28	0.003	7.992	4.447	5.853	0.002	0.003	0.007	0.000	0.013	0.024	1.567	0.000	19.912	0.836
DC0245 Amp pblast	2.85	12.9	14.22	40.0	0.47	12.01	0.50	0.08	0.20	12.41	-	95.70	23	0.838	2.912	2.540	6.068	0.090	1.950	0.057	0.000	0.010	0.026	1.574	0.000	16.064	0.649
DC0245 Chl	0.00	26.4	21.11	28.7	0.01	0.01	0.04	0.10	0.16	10.32	-	87.02	28	0.001	7.710	4.867	5.618	0.003	0.003	0.005	0.000	0.015	0.027	1.689	0.000	19.938	0.820
DC0245 Amp corv	0.01	24.0	20.16	27.5	0.01	0.08	0.05	0.05	0.19	13.75	-	85.79	28	0.004	7.231	4.814	5.570	0.003	0.017	0.007	0.000	0.008	0.032	2.330	0.000	20.016	0.756
Antigorite-Talc-Olivine Schists																											
DC0238 Ol		45.3	0.01	39.9	-	0.01	-	0.00	0.31	13.74	0.40	99.67	4	0.000	1.695	0.000	1.001	0.000	0.000	0.000	0.000	0.000	0.007	0.289	0.008	2.999	0.855
DC0238 Tlc	0.01	37.4	1.05	44.4	0.01	0.02	0.02	0.25	0.04	4.38	-	87.51	28	0.004	10.373	0.230	8.263	0.003	0.004	0.002	0.000	0.037	0.006	0.682	0.000	19.604	0.938
DC0238 Chl	0.05	28.3	0.02	38.5	0.03	0.18	0.01	0.02	0.24	11.70	-	79.12	28	0.021	9.111	0.005	8.322	0.008	0.041	0.002	0.000	0.004	0.045	2.126	0.000	19.686	0.812
DC0238 Trem	0.24	23.1	0.16	57.0	0.06	12.72	0.03	0.04	0.11	2.73	-	96.26	23	0.064	4.796	0.026	7.943	0.010	1.899	0.004	0.000	0.004	0.013	0.318	0.000	15.076	0.938
DC0238 Sp		1.6	0.15	0.2		0.00	1.28	15.14	0.24	74.01	-	92.68	4	0.000	0.111	0.008	0.009	0.000	0.000	0.045	0.002	0.563	0.010	2.909	0.000	3.659	0.037
GS1013 Ol	0.02	49.6	0.00	40.8	0.03	0.00	0.00	0.00	0.12	9.07	0.32	99.95	4	0.000	1.910	0.000	1.054	0.000	0.000	0.000	0.000	0.000	0.003	0.196	0.006	3.169	0.907
GS1013 Opx	0.01	34.7	0.20	57.6	0.01	0.20	0.05	0.01	0.19	6.33	-	99.34	6	0.001	1.792	0.008	1.998	0.000	0.007	0.001	0.000	0.000	0.006	0.184	0.000	3.997	0.907
GS1013 Tlc	0.02	30.8	0.13	60.5	0.00	0.23	0.01	0.01	0.18	6.70	-	98.61	22	0.006	5.831	0.020	7.685	0.000	0.032	0.001	0.000	0.001	0.020	0.712	0.000	14.307	0.891
GS1013 Ilm	-	6.2	0.00	0.0	-	0.01	54.91	0.13	0.77	38.03	-	100.08	3	0.000	0.223	0.000	0.001	0.000	0.000	0.995	0.000	0.002	0.016	0.766	0.000	2.003	0.225
GS01013 rut	-	0.0	0.00	0.0	-	0.00	96.34	0.41	0.00	0.54	-	97.32	3	0.000	0.001	0.000	0.000	0.000	0.000	1.490	0.000	0.007	0.000	0.009	0.000	1.507	0.064

Table 2 - Major and trace element chemistry of samples*

	Ultramafic Rocks														Mafic Rocks			
sample	**GS01-011**	**GS01-012d**	**GS01-012**	**GS01-013**	**GS01-018**	**GS01-019**	**DC0238**	**DC0239**	**DC0240**	**DC0241**	**DC0242**	**DC0243**	**DC0244**	**DC0247**	**DC0246**	**DC0231**	**DC0235**	**DC0245**
SiO2	49.5	46.1	46.3	46.3	42.9	48.0	48.2	47.8	48.2	48.4	48.1	47.6	47.4	48.0	52.9	48.9	44.6	33.1
TiO2	0.04	1.23	1.23	0.07	0.03	0.04	0.03	0.02	0.02	0.02	0.02	0.03	0.02	0.02	0.26	0.35	0.49	0.82
Al2O3	1.91	1.81	1.80	3.23	0.47	1.67	1.13	0.81	1.00	0.73	0.79	2.71	0.89	1.72	3.97	2.19	9.46	20.39
FeO*	7.04	8.35	8.29	7.91	9.50	7.37	7.45	7.85	7.84	7.04	7.51	8.73	7.91	7.51	3.83	11.59	11.17	14.06
MnO	0.10	0.15	0.15	0.12	0.13	0.12	0.09	0.10	0.09	0.10	0.09	0.14	0.10	0.11	0.12	0.19	0.17	0.21
MgO	41.2	41.5	41.3	42.2	46.2	42.6	42.9	43.2	42.7	43.6	43.4	40.7	43.4	41.3	28.3	20.7	19.0	26.0
CaO	0.05	0.50	0.49	0.05	0.71	0.12	0.06	0.08	0.04	0.08	0.06	0.12	0.15	0.14	10.03	14.43	12.45	3.06
Na2O	0.10	0.09	0.15	0.10	0.11	0.09	0.16	0.07	0.13	0.04	0.06	0.04	0.03		0.03	0.15	1.26	0.55
K2O	0.01	0.01	0.01	0.01	0.01	0.01	0.01	0.01	0.01	0.01	0.01	0.01	0.01	0.01	0.02	0.03	0.17	0.14
P2O5	0.02	0.30	0.31	0.02	0.01	0.02	0.01	0.01	0.01	0.01	0.00	0.00	0.00					
L.O.I.	6.09	4.62	4.48	6.17	4.77	6.18	8.92	8.10	8.42	8.48	8.07	8.04	9.59	9.17	5.56	2.72	3.48	9.11
Mg#	0.91	0.90	0.90	0.90	0.90	0.91	0.91	0.91	0.91	0.92	0.91	0.89	0.91	0.91	0.93	0.76	0.75	0.77
C	1300	805	808	2510	1820	905	-	-	-	-	-	-	-	-	-	-	-	-
S	-	-	-	-	-	-	36	61	61	91	99	44	137	-	2	-	44	18
Co	96	95	121	99	113	104	111	108	108	104	109	104	102	99	44	66	74	120
Ni	2018	1472	1688	2085	2203	2248	2245	2194	2166	2177	2200	2174	2098	2174	395	688	311	664
Cu	3.5		2.9	3.1	20.4	3.6	12.5	14.5	9.0	16.5	15.1	6.3	20.8	1.9	1.7	20.4	4.9	2.0
Zn	42.6	37.5	38.9	33.7	47.4	46.9	40.9	43.4	46.2	39.0	45.5	56.3	46.7	44.2	20.0	35.7	39.8	79.5
Ti	236	6960	6452	308	41	140	125	67	72	54	58	88	68	76	1420	1990	2887	4100
Cr	2262	1244	1521	2101	3123	2591	2987	2747	2847	2129	3048	2442	2853	2376	59	787	370	320
Li	11.7	10.0	7.9	6.5	2.8	6.1	5.9	0.8	0.9	1.0	1.5	3.2	0.8	2.2	0.4	4.1	9.1	11.3
Sc	8.0	11.5	11.6	9.5	7.3	6.2	4.1	3.1	2.1	6.1	1.6	0.6	4.6	2.2	2.0	33.5	9.6	24.8
V	24	25	31	31	29	30	28	25	28	19	21	49	33	31	28	197	407	170
Rb	0.46	0.26	0.09	0.35	0.27	0.29	0.07	0.06	0.09	0.42	0.06	0.31	0.07	0.21	0.06	0.11	0.41	0.30
Sr	7.91	22.97	23.11	6.73	25.89	6.86	1.72	1.50	1.27	2.28	1.99	2.26	4.75	3.48	3.90	68.42	112.60	49.58
Y	1.51	12.92	13.44	1.10	1.63	0.42	0.71	0.26	0.37	0.23	0.32	2.97	0.31	2.03	18.89	33.33	26.29	14.72
Zr	2.52	16.63	12.63	0.34	1.68	1.51	0.18	0.31	0.17	0.16	0.14	0.46	0.12	0.44	29.04	6.65	13.27	5.83
Nb	1.40	25.90	21.53	1.22	0.98	0.72	0.31	0.26	0.18	0.24	0.20	0.38	0.12	0.34	10.71	3.87	7.51	7.08
Ba	1.52	0.53	0.37	0.69	0.53	0.36	0.88	4.34	2.59	2.13	2.40	3.78	0.99	6.06	1.90	4.54	24.87	24.47
La	0.484	3.843	2.659	0.198	0.650	0.201	0.100	0.176	0.190	0.159	0.139	0.685	0.258	0.604	17.245	9.602	6.049	7.809
Ce	1.207	11.629	8.874	0.481	1.438	0.385	0.264	0.296	0.354	0.276	0.264	1.574	0.426	1.379	39.345	22.007	13.428	16.238
Pr	0.167	1.872	1.379	0.066	0.185	0.044	0.039	0.030	0.039	0.030	0.029	0.205	0.040	0.197	4.342	3.102	1.858	2.003
Nd	0.721	8.926	6.692	0.232	0.759	0.165	0.188	0.113	0.147	0.096	0.111	0.906	0.140	0.879	15.818	14.640	8.932	8.382
Sm	0.174	2.560	2.131	0.073	0.173	0.040	0.063	0.021	0.030	0.021	0.022	0.234	0.030	0.208	2.994	4.211	2.827	2.062
Eu	0.024	0.371	0.306	0.011	0.046	0.024	0.016	0.006	0.006	0.007	0.005	0.015	0.006	0.017	0.820	1.087	1.230	0.667
Gd	0.226	3.038	2.830	0.076	0.219	0.048	0.076	0.026	0.035	0.025	0.029	0.298	0.033	0.243	2.982	4.928	3.660	2.408
Tb	0.041	0.508	0.385	0.019	0.038	0.008	0.014	0.004	0.007	0.004	0.005	0.056	0.006	0.043	0.486	0.887	0.688	0.414
Dy	0.248	2.720	2.412	0.135	0.228	0.058	0.097	0.031	0.044	0.026	0.036	0.389	0.040	0.275	2.960	5.620	4.533	2.630
Ho	0.058	0.554	0.465	0.041	0.057	0.015	0.023	0.007	0.011	0.007	0.010	0.098	0.009	0.062	0.600	1.153	0.942	0.545
Er	0.192	1.415	1.358	0.179	0.190	0.069	0.081	0.029	0.039	0.026	0.036	0.339	0.032	0.196	1.778	3.351	2.741	1.608
Tm	0.032	0.180	0.171	0.043	0.031	0.013	0.015	0.006	0.008	0.005	0.007	0.061	0.006	0.033	0.271	0.497	0.423	0.242
Yb	0.242	0.903	0.909	0.391	0.201	0.140	0.114	0.050	0.063	0.043	0.056	0.448	0.048	0.221	1.669	3.129	2.708	1.497
Lu	0.049	0.128	0.136	0.100	0.032	0.034	0.021	0.010	0.012	0.008	0.010	0.074	0.007	0.033	0.217	0.449	0.385	0.198
Hf	0.084	0.414	0.306	0.029	0.079	0.051	0.014	0.016	0.013	0.008	0.010	0.030	0.009	0.024	1.005	0.457	0.614	0.278
Ta	0.101	1.947	1.543	0.061	0.028	0.035	0.027	0.017	0.013	0.014	0.015	0.078	0.009	0.049	1.013	0.230	0.366	0.317
Pb	0.06	0.10	0.03	0.06	0.09	0.08	0.10	0.14	0.13	0.14	0.15	0.27	0.13	0.26	0.71	0.97	1.02	0.61
Th	0.16	0.62	0.38	0.15	0.13	0.13	0.05	0.05	0.06	0.04	0.05	0.25	0.05	0.10	1.78	0.58	0.39	0.38
U	0.10	1.00	0.72	0.23	0.03	0.05	0.05	0.04	0.03	0.04	0.04	0.16	0.02	0.10	0.51	0.11	0.15	0.05

* Major elements by XRF, trace lements by ICPMS, C and S by Leco. Major elements normalized to 100% anhydrous.

Table 3. U-Pb Results for ultramafic sample

Description of Fractions	Weight (mg)	U (ppm)	Th (ppm)	Pb (ppm)	Th/U	TCPb (pg)	$^{206}Pb/^{204}Pb$	$^{206}Pb/^{238}U$	$^{207}Pb/^{235}U$	$^{207}Pb/^{206}Pb$	Model Ages (Ma) $^{206}Pb/^{238}U$	$^{207}Pb/^{235}U$	$^{207}Pb/^{206}Pb$	%Disc
GS01-012														
1 z, lt yell frags 20NM (11)	59	76	27	2.8	0.36	25	380	0.03184±9	0.2229±15	0.05078±33	202.1±0.6	204.4±1.2	231.1±15.0	12.8
2 z, col to lt yell shards 20NM (10)	87	88	4	3.8	0.04	5	3881	0.04322±5	0.4757±6	0.07983±7	272.8±0.3	395.1±0.4	1192.8±1.6	78.7
3 z, lt yell large irreg frags 20NM (12)	72	80	5	2.9	0.07	27	440	0.03213±4	0.2819±10	0.06362±22	203.9±0.2	252.1±0.8	729.1±7.3	73.2

z: zircon, col: colourless number in parentheses corresponds to the total number of grains analysed.
0NM refers to a non-magnetic mineral fraction on a Frantz Isodynamic Separator with a 0 degree side tilt.
All errors in this table reported at 1 sigma.